https://ntrs.nasa.gov/search.jsp?R=19810004891 2020-03-21T14:51:47+00:00Z

N O T I C E

THIS DOCUMENT HAS BEEN REPRODUCED FROM MICROFICHE. ALTHOUGH IT IS RECOGNIZED THAT CERTAIN PORTIONS ARE ILLEGIBLE, IT IS BEING RELEASED IN THE INTEREST OF MAKING AVAILABLE AS MUCH INFORMATION AS POSSIBLE

...de available under NASA sponsorship
the in... dis-
...eminat... Survey
Program ...out liability
...for any use ...or"

centro studi ed applicazioni
in tecnologie avanzate - bari
BARI - VIA GIOVANNI AMENDOLA, 173

81-10041
CR-163751

(E81-10041) SCALE EFFECTS: HCMM DATA SIMULATION. USAGE OF FILTERING TECHNIQUES FOR SCALING-UP SIMULATIONS (Centro Studi ed Applicazioni in Tecnologie) 63 p
HC A04/MF A01

N81-13402

CSCL 08B G3/43

Unclas
00041

RECEIVED
NOV 5 1980
SIS/902.6
HCM-035
Type II

SCALE EFFECTS: HCMM DATA SIMULATION

Usage of filtering techniques for scaling-up simulations

Contract CSATA-JRC Ispra n. 960-78-10 SISP I

Original photography may be purchased from:
EROS Data Center
Sioux Falls, SD 57198

INDEX

... may be purchased from
... with:

... Falls, SD

1. INTRODUCTION

It is well known that the gray level of image's pixels depends on the radiance coming, in a particular spectral range, from the ground areas corresponding to the pixels. If each area is homogeneous no problem exists in its interpretation; if, on the contrary, a lot of different objects are contained, they contribute in different manners to the global gray level of the pixel.

The problem becomes more important as greater dimension pixels are involved, i.e. the problem must to be faced to understand the informative content of the data.

Images from HCMM are typical example of this with their pixels 500 x 500 m^2 dimensioned. It is then necessary to study the so called scale effect to understand how detailed informations aggregate to give rise to low or very low resolution data as they are detected for example from a high altitude platform.

The first question to which this work was devoted was the simulation of HCMM data starting from better resolution ones.

The following approach was however adopted:

- determine a methodology which permits the correlation of different resolution data;
- test the methodology for the simulation of little altitude increase (usage of aircraft data);
- simulate if possible HCMM images.

The methodology is based on filtering techniques in the hyphothesis that all changes due to altitude increase can be represented by a point spread function. These aspects, together with a "practical" introduction to the filtering technique, are particularly pointed out all along the work. As will be seen, no attempt is made however to simulate HCMM data; attention is mainly focused on the scale effect in its general aspects also for its importance in problems such as registration between images and so on.

2. SCALE EFFECT: THEORETICAL MODEL

2.1. Possible reduction methods

At first sight the simulation of an altitude increase of acquisition platform consists of an image's reduction and this is equivalent to a suitable smoothing. This can be achieved by two methods:

a) neighhorhood averaging techniques
b) filtering techniques

a) Neighborhood averaging techniques. These consist, as it's well known, in an arithmetical or weighted average of the gray values on a number of pixels equal to reduction factor (for example 4x4 pixels if the reduction factor is 16:1).

b) Filtering techniques. If this operation is realized in the spatial domain, it consists of the convolution of the image with the weights mask and then of the decimation of the points according to the appropriate scale factor.

It's interesting to note that the former approach can be viewed as a particular case of the filtering technique where the filter dimensions are equal to the reduction factor. In this case the two steps of convolution and decimation give an output equal to the averaging approach output.

In both cases the weights mask has the role of a point-spread function (PSF) (for a survey on PSF and MTF see appendix 1) so its shape (and hence the MTF shape) should represent the physical characteristics of the process.

The averaging approach is certainly very convenient from a computer time point of view, but it is considerably limited for accurate simulations. The weights mask must have in fact a Fourier transform as similar as possible to the process itself MTF. Since the more PSF samples there are, the better the transform shape can be controlled, it is convenient to use large dimensioned masks. In averaging technique, however, mask dimensions are fixed by the scale factor so that for little reductions very little extent mask must be used with the consequent impossibility of controlling the MTF shape.

2.2. Discrete image formation process

To understand how the function simulating a scaling up can be obtained, it is convenient to examine the mathematical processes generating discrete images. In a general manner, the imaging process at the two altitudes can be briefly represented as in Fig. 2.1.

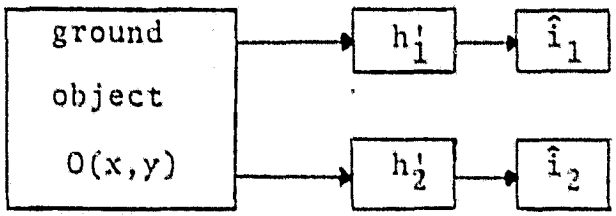

Fig. 2.1

where $\hat{i}_1$ is the discrete image at lower altitude q_1

$\hat{i}_2$ is the discrete image at higher altitude $q_2 = Kq_1$ $(K > 1)$

h_1' is the global PSF for image formation at altitude q_1

h_2' is the global PSF for image formation at altitude $q_2 = Kq_1$ $(K > 1)$

This means that the same ground object is seen in different manners (i.e. with different PSFs) and so different images are obtained.

Fig. 2.2. shows a more detailed representation of discrete image formation process.

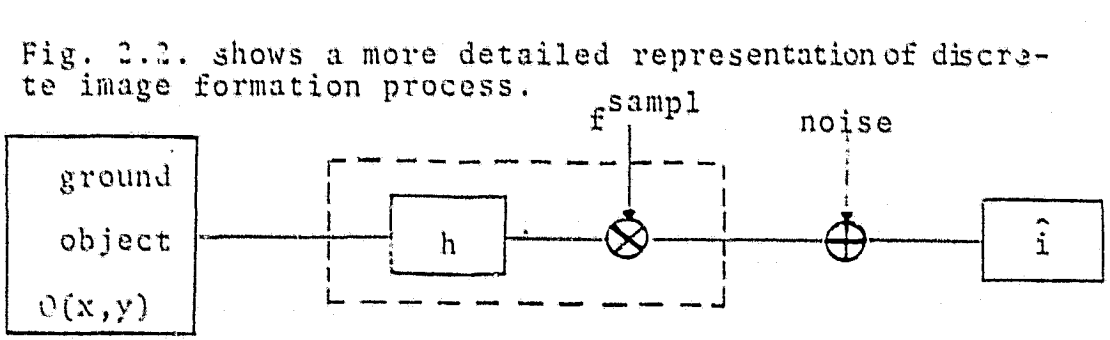

Fig. 2.2.

i.e. each PSF is seen as composed of a continuous PSF followed by a sampler.

The assumption is made that the signal-to-noise ratio value is sufficiently high so that the noise can be ignored.

It's interesting to carry out a graphical derivation (in one-dimensional form) of the process.

The assumption is made that SIPSF are involved so that the degrading process can in the same way be represented by its MTF.

The ground object corresponding to the image being considered is represented by the function $o(x)$ (Fig. 2.3) while it is assumed that the continuous PSF h_1 of Fig. 2.2 is given by Fig. 2.3b. The integration performed on the photodetector surface is mathematically represented by the convolution of $o(x)$ with $h_1(x)$ (i.e. the multiplication of $O(f)$ and $H_1(f)$ (Fig. 2.3c)(*).

The assumption can be made that the convolution output has its spatial frequency content limited to a f_M^1 frequency. The filtered image is then spatially sampled. The assumption can be made that the sampling system works so that the image has neither overlaps nor gaps between pixels. Referring, for example, to the scan in the flight direction, this condition is satisfied by the frequency [Ref. 1] .

$$f_S = \frac{V/h}{n\alpha}$$

Where

V = Platform velocity

h = Platform altitude

n = Number of sensors

(*) It must be noted that the object function $o(x)$ is obtained by means of truncation of an extended ground object function with a window function which is unity in the range T_0 and zero elsewhere. This is equivalent to convolve the object transform with the window transform (i.e. a $\frac{\sin x}{x}$ function and this introduces a certain amount of ripple; this is however, disregarded in this treatment).

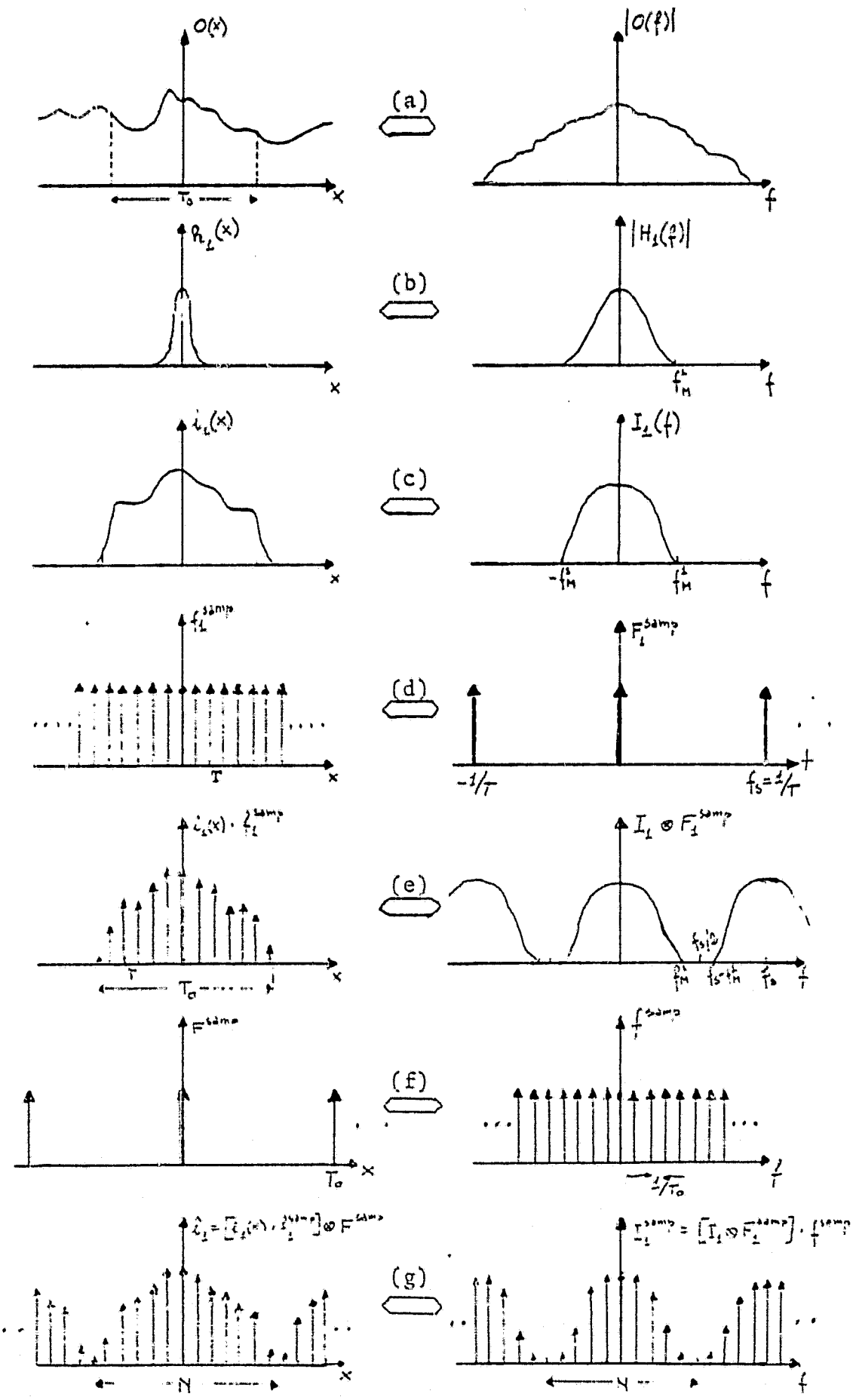
O(x)
|O(f)|
(a)
T₀
x
f
h_L(x)
|H_L(f)|
(b)
f_M^L
i_L(x)
I_L(f)
(c)
-f_M^L
f_M^L
f_L^samp
F_L^samp
(d)
T
-1/T
f_s=1/T
i_L(x) · f_L^samp
I_L ⊗ F_L^samp
(e)
f_s-f_M^L
F^samp
f^samp
(f)
T₀
1/T₀
Î_L = [i_L(x) · f_L^samp] ⊗ F^samp
I_L^samp = [I_L ⊗ F_L^samp] · f^samp
(g)
N

fig. 2.3

α = Istantaneous field of view(IFOV)

With this assumption and supposing the sampler is an ideal Dirac delta function, it can be written

$$f^{samp} = \sum_{j=-\infty}^{+\infty} \delta(x-j\ \Delta x_{sampl}) \qquad (1)$$

where Δx_{sampl} is the pixel dimension depending on the altitude and system IFOV. It is assumed that for q_1 altitude $\Delta x_{sampl} = T$ (See Fig. 2.3d).

As it is stated in Fig. A.I.2 the sampling is equivalent to a multiplication in space domain, i.e. a convolution in frequency domain. The result is shown in Fig. 2.3e. It must be noted that if the folding frequency ($f_s/2$) is less than f_{N_1} (i.e. if data are undersampled), the aliasing phenomenon appears.

To provide a mapping between transform domain and image space and to permit transformed data to be handled by computer, it is necessary to discretize also Fourier domain. The so-called Discrete Fourier Transform (DFT) is accomplished by sampling the continuous Fourier transform by means of a f^{samp} with $1/T_o$ frequency step (Fig. 2.3f); this produces the iteration of the space signal as it appears from Fig. 2.3g. For the two-dimensional case, this periodicity is equivalent to the situation depicted in Fig. 2.4.

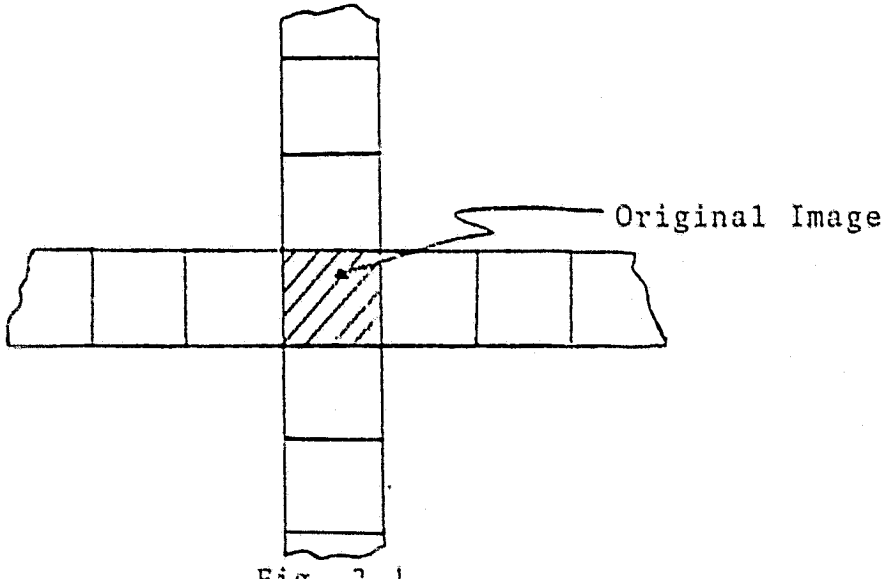

Fig. 2.4

From this it follows [Ref. 2, pg. 20] that when finite extent discrete arrays are convolved, "circular convolution" must be used.

It must be noted that in the frequency domain a number of samples is generated equal to spatial domain one (for primary components). This number is obviously $N = T_o/T$.

The same graphical derivation can be carried out for upper altitude (q_2) image, i_2. The input (ground object $o(x)$) is the same than in Fig. 2.3a. Generally the acquisition system is a different one so a new PSF, $h_2(x)$, is now involved; referring to the case of a loss of resolution, the width of its non-zero region is however greater than the lower altitude one.

In the particular case the acquisition system is the same, the upper altitude PSF can be assumed to be carried out only by means of geometrical properties; other effects due to altitude increase (just like atmospheric effects, etc.) are not taken into account. In this hypothesis the time-scaling relation is used [Ref. 3 pg. 32] i.e. if K is the altitude factor then

$$h_2(x) = h_1(x/K)$$
$$H_2(f) = KH_1(Kf) \qquad (2)$$

If the two altitudes are double the other, the $h_2(x)$ can be represented as in Fig. 2.5b where $f_M^2 = 1/2\, f_M^1$; Fig. 2.5c shows the convolution of this PSF with ground object.

Also the pixel dimensions are obtained by means of the scaling of the lower altitude pixel, i.e. now $\Delta x_{sampl} = 2T$, as it can be seen in Fig. 2.5a; the result of the sampling is represented in Fig. 2.5e. It's obvious that now the samples' number is the half of the lower altitude one. The step corresponding to Fig. 2.5f and Fig. 2.5g is equivalent to that seen in Fig. 2.3f and 2.3g.

It must be noted that in the frequency domain the sampling spacing is the same as for lower altitude (i.e. $1/T_o$) while the samples number is reduced, as for space samples, to a half.

2.3. Determination of a scale-change function.

A Fourier transform pair $g \leftrightarrow \mathcal{G}$ which permits one to carry out i_2 directly from $\hat{i}_1$ must be defined. This pair must satisfy the relations

$$\mathcal{I}_2 = \mathcal{I}_1 \cdot \mathcal{G} \tag{3a}$$

$$\hat{i}_2 = \hat{i}_1 \otimes g \tag{3b}$$

Where with $\mathcal{I}_1(\mathcal{I}_2)$ is denoted the DFT of $\hat{i}_1(\hat{i}_2)$ i.e. a complex function. It immediately appears that such a determination can be easily made in frequency domain. In fact if

$$\begin{aligned} \mathcal{I}_1(u.v) &= I_1(u,v) \exp\left[i\,\psi(u,v)\right] \\ \mathcal{I}_2(u,v) &= I_2(u,v) \exp\left[i\,\phi(u,v)\right] \\ \mathcal{G}(u,v) &= G(u,v) \exp\left[i\,\rho(u,v)\right] \end{aligned} \tag{4}$$

Solving the equation (3a) gives $\mathcal{G}(u,v) = G(u,v) \exp\left[i\,\rho(u,v)\right]$ where

$$\begin{aligned} G(u,v) &= I_2(u,v)/I_1(u,v) \\ \rho(u,v) &= \phi(u,v) - \psi(u,v) \end{aligned} \tag{5}$$

Liv and Gallangher [Ref. 4] give a detailed description of the problems involved in minimizing the error between $\mathcal{I}_2$ and $\mathcal{I}_1$-$\mathcal{G}$ functions. The main problems concern $\hat{i}_1$ and $\hat{i}_2$ phases choice; in the present form phases are, however, neglected so that the model is restricted to magnitude values, i.e.

$$G = G(u,v) = I_2(u,v)/I_1(u,v) = I_2^{sampl}/I_1^{sampl} \tag{6}$$

It is not so easy to solve equation (3b) if an operation inverse to the convolution were to be used.

In order to realize a significative comparison, the same number of samples, for the two altitudes spectra, should

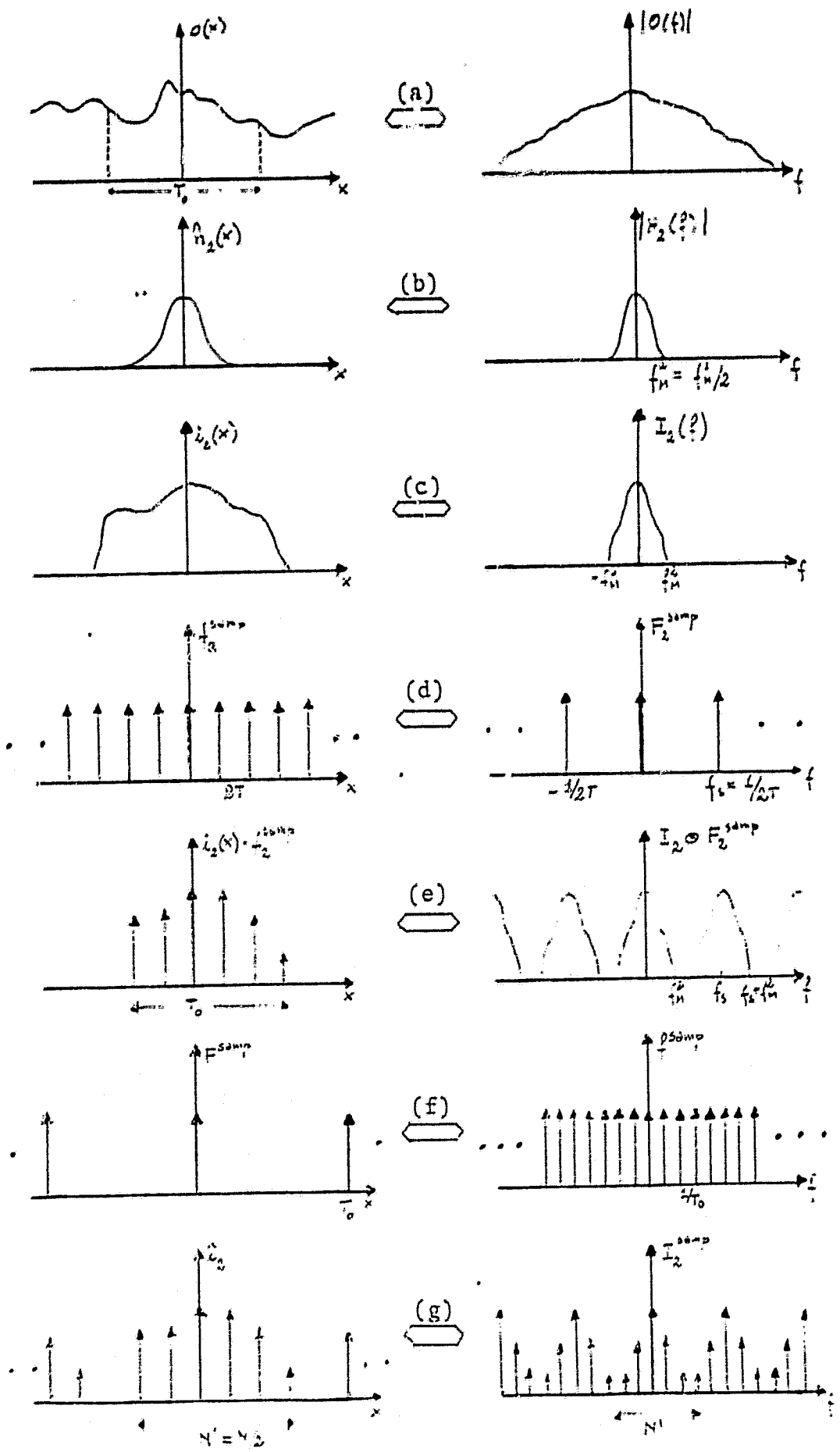
o(x)
|O(f)|
(a)
T_0
x
f
$\hat{n}_2(x)$
$|N_2(f)|$
(b)
$f_M' = f_M'/2$
$i_2(x)$
$I_2(f)$
(c)
$-f_M'$
f_M'
$\hat{i}_2^{samp}$
F_2^{samp}
(d)
ΔT
$-1/2T$
$f_s = 1/2T$
$i_2(x) \cdot \hat{i}_2^{samp}$
$I_2 \circledast F_2^{samp}$
(e)
T_0
$-f_M'$
f_s
$f_s - f_M'$
F^{samp}
ρ^{samp}
(f)
$1/T_0$
$\hat{i}_2$
I_2^{samp}
(g)
$N' = N_2$
N'

fig. 2.5

be used. Because I_2^{sampl} has the primary component with N' samples, it's convenients to enlarge it up to N samples by adding zeros. Then the spectra to be compared are shown in Fig. 2.6.

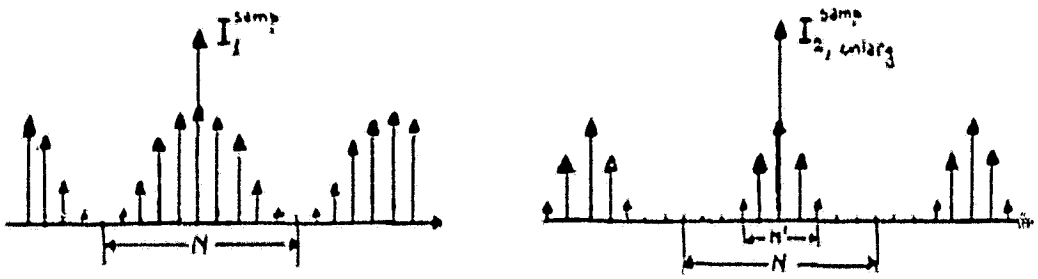

fig. 2.6

It must be noted that this enlargement has no consequences because the meaningful part of the spectrum remains unchanged; the spatial domain image is also enlarged but without any add of information.

Referring to the primary component N samples, it's possible to write

$$\begin{aligned} I_{2,enlarg}^{sampl} &= O(f) \cdot H_2(f) \cdot f^{samp} \\ I_1^{sampl} &= O(f) \cdot H_1(f) \cdot f^{samp} \end{aligned} \qquad (7)$$

so it is true that

$$G = \frac{I_{2,enlarg}^{sampl}}{I_1^{sampl}} = \frac{H_2'(f)}{H_1'(f)} \qquad (8)$$

where $H'_{1,2}(f) = H_{1,2}\, f^{samp}$ (9)

is the acquisition system continuous MTF sampled with $1/T_o$ step.

The expression (8) states clearly that the G function can be carried out either directly from the data or from information on the acquisition system.

Since spatial filters are passive devices, they don't amplify the signal. The G function, then must satisfy the constraint

$$G(u,v) \leq 1$$

While this must be tested for different sensors, it is automatically true when H_2 is carried out by the scaling of H_1; this also prevents any problem coming from H_1 zeros.

The g function is obtained by means of the Inverse Discrete Fourier Transform (IDFT). This g is constituted of N samples, but only few of them are non-zero.

Before applying the proposed method for a generical scaling-up, it is better to verify it by performing the filtering in order to re-obtain $\hat{i}_2$ starting from $\hat{i}_1$. This operation can be performed either in the spatial or in the frequency domain.

In the latter one, I_2^{sampl} to be re-obtained, the multiplication of G and I_1^{sampl} must be realized. This gives, however, $I_{2,enlarg}^{sampl}$ so it's necessary to reduce

it by dropping (N-N')/2 zero value points at each edge.

The filtering in the spatial domain is obtained convolving $\hat{i}_1$ with the g samples. The output consists of N samples T spaced whose spectrum is just $I_{2,enlarg}^{sampl}$. If a decimation of samples is made with a factor K equal to the scale factor (in the particular case of § 2.2 K = 2), I_2^{samp} is just obtained.

The decimation is in fact equivalent to the convolution in the frequency domain with a pulse train, spaced 1/KT.

This produces a loss of a part of the spectrum due to the aliasing; this part is however just the one containing zero values so the final result is similar to Fig. 2.5g.

It must be osserved that the considered model is based on the assumption of the existence of a unique MTF for each altitude, i.e. in the hyphothesis of shift-invariant PSF. If this is not true, the model is no longer applicable in its present form.

3. SCALE EFFECT: OPERATIVE APPROACH.

The problems involved in the simulation of a higher altitude image are:

- determine the appropriate scale change filter
- perform the filtering operation.

3.1 Determination of the scale change filter.

To solve the problem with a deterministic approach it is necessary no longer to consider data and to use only a priori informations. Referring to expression (8) the G filter can be carried out by means of ratioing discrete MTFs.

This obviously requires the exact knowledge of transfer function at each altitude; if these are not known, they must be constructed from the knowledge of imaging process, of all degradation sources involved and of their models.

A quick survey of the principal degradations of an acquisition system is reported in appendix II, but it appears evident that it's a very hard job to use this approach for carrying out the global transfer function on the assumption, however, that the lower altitude MTF is known and if the image seen at upper altitude bu the same acquisition system is desired, it is possible to arrive easily at the G function.

According, in fact, to (2), the G filter project procedure can be schemed as in Fig. 3.1.

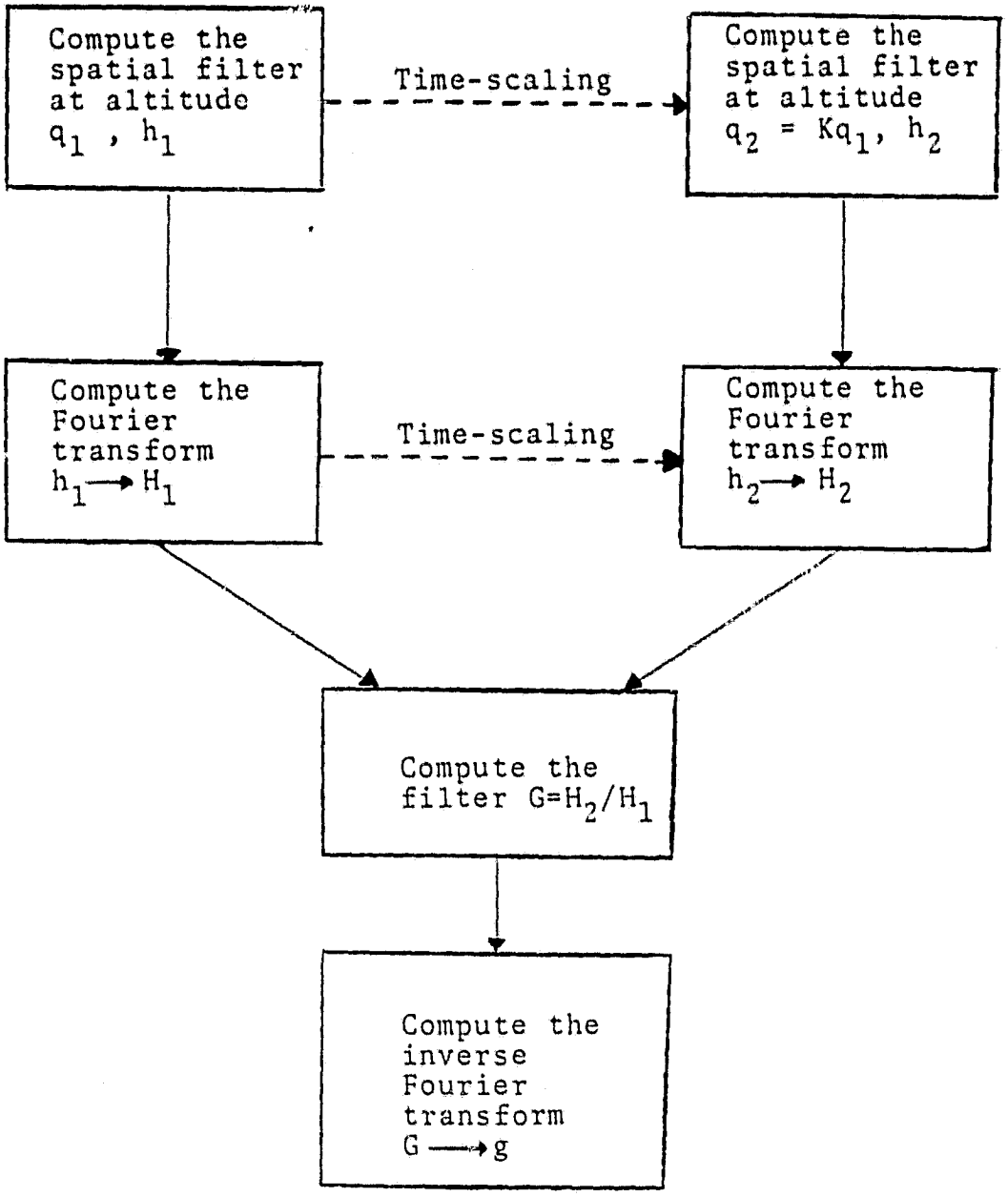
Compute the spatial filter at altitude q_1 , h_1
Time-scaling
Compute the spatial filter at altitude $q_2 = Kq_1$, h_2
Compute the Fourier transform $h_1 \longrightarrow H_1$
Time-scaling
Compute the Fourier transform $h_2 \longrightarrow H_2$
Compute the filter $G=H_2/H_1$
Compute the inverse Fourier transform $G \longrightarrow g$

Fig. 3.1

It must be noted that the time-scaling property can be indifferently applied either in space domain or in the frequency domain.

The meaning of the operation $G=H_2/H_1$ is that explained in § 2.3.

Neglecting the phase term, the function

$$G_{m,n} = \begin{cases} \dfrac{H_{2m,n}}{H_{1m,n}} & \text{if} \quad \dfrac{H_{2m,n}}{H_{1m,n}} < 1 \\ 1 & \text{if} \quad \dfrac{H_{2m,n}}{H_{1m,n}} > 1 \end{cases} \qquad (10)$$

is computed.

If the modulation transfer function informations are not available, the scale change filter must be evaluated directly from the data.

According to expression (6) the empirical approach is realized by ratioing the two altitudes images' spectra.

In order for the use of the Fourier techniques to be meaningful, it is necessary to remove from the images all the shift-variant effects. Apart from the eventual SVPSF components of the acquisition system, there are some standard SV effects related to the acquisition itself. The actual procedure should consist in a deconvolution for these SVPSF, but empirical methods are usually used to correct data.

In a first approximation two kinds of effects must be eliminated. The first is the so-called panoramic effect. This is due to the variation of the ground resolution when the view angle is changed (see Fig. 3.2).

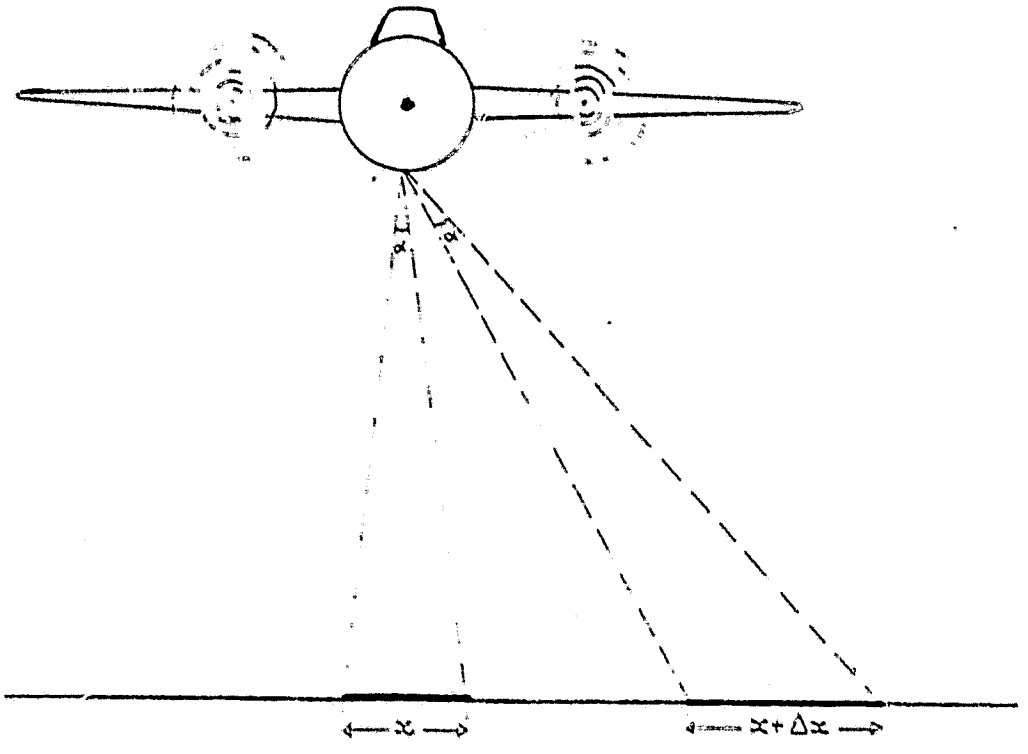

Fig. 3.2

If this geometrical effect is left uncorrected, it gives incorrect spatial frequency values, especially for aircraft data where panoramic effect is more relevant. The correction can be done by using resampling techniques which obviously yield an increase of samples number in the direction normal to flight line.

Another effect depending on the position in the image plane is that due to the different atmospheric thickness for nadir and off-nadir observations. This yields a symmetrical lowering of the values at images edges respect to actual values.

Instead of deconvolution approach, this effect can be statistically corrected by means of best-fit techniques. The assumption is made that for almost uniform regions in the image, the profile of the average values of the columns in this region can be fitted with a second order polynomial.

An example of this kind of correction is reported in Fig. 3.3 and in Fig. 3.4. The first shows a corrected and an uncorrected 3000m aircraft image, while Fig. 3.4 shows the profiles of average values of the columns (averaged on a number of lines). Actually there are two competing atmospheric effects present in remote sensed data [Ref. 5] . The first is the attenuation which reduces the magnitude of sensed radiation. The second is an active effect represented by scattering and/or emission. The balance between them depends on the direction of scan relative to the sun's position. If the scanner looks toward the sun, the dominant effect is the attenuating one. The opposite effect dominates if the scanner looks away from the sun. It follows that the proposed correction isn't completely exhaustive while a third-order curve should be necessary for a better correction; no attempt has however been made.

Another effect is that coming from atmospheric thickness increase due to platform altitude increase. As it follows from [Ref. 6] to simulate the increase of optical thickness, a linear transformation can be used which is independent from starting haze level, but dependent on added layer. It can then be considered shift-invariant and nothing has been done to take it into account.

When all known shift-variant effects have been removed both from lower and upper altitude images, Fourier techniques can be applied (in the assumption of SIPSF of the instrument).

In the following step Fourier transform of "corrected" images at different altitudes must be calculated.

Given a discrete image in the form of the finite sequence $\{i(n_1,n_2)\}$ $n_1 = 0,\ldots,N-1, n_2 = 0,\ldots,N-1$ its two-dimensional discrete Fourier transform is obtained [Ref. 7; Ref. 8] as the z-transform along the two circles $z_1=e^{j\omega_1}$, $z_2=e^{j\omega_2}$ so that the transform is

$$I(k_1,k_2)=I(z_1,z_2)\Big|_{z_1=\exp\left[j(2\pi k_1/N)\right]\ ,\ z_2=\exp\left[j(2\pi k_2/N)\right]} =$$

$$= \sum_{n_1=0}^{N-1}\sum_{n_2=0}^{N-1} i(n_1,n_2)\exp\left[-j(2\pi k_1 n_1/N)\right]\exp\left[-j(2\pi k_2 n_2/N)\right]$$

with $k_1=0,\ldots,N-1$, $k_2=0,\ldots,N-1$

From an implementation point of view this two-dimensional transform is obtained by performing two one-dimensional transform as is shown in Fig. 3.5.

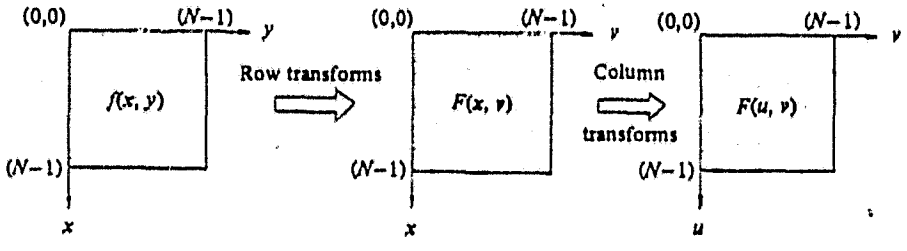

Fig. 3.5

It must be noted that the result has a phase which is such that the meaningful parts of the transform are at the corners of the display. To help visual examination of the transform, it's convenient to shift the origin in the center of the N x N points frequency domain. This is obtained either by re-ordering transform coefficients or by making use of the translation property of Fourier transform pair

$$f(x,y)\ \exp\left[\, j2\pi(u_o x+v_o y)/N\right] \Longleftrightarrow F(u-u_o,v-v_o)$$

i.e. (12)

$$i(n_1,n_2)\ \exp\left[\, j(2\pi k_1 n_1/N)\right]\ \exp\left[j2\pi k_2 n_2/N)\right] \Longleftrightarrow \delta(m_1-k_1,m_2-k_2)$$

If the shift is $k_1=k_2=N/2$ then

$$\exp\left[\, j2\pi(k_1 n_1+k_2 n_2)/N\right] = e^{j\pi(n_1+n_2)} = (-1)^{n_1+n_2} \qquad (13)$$

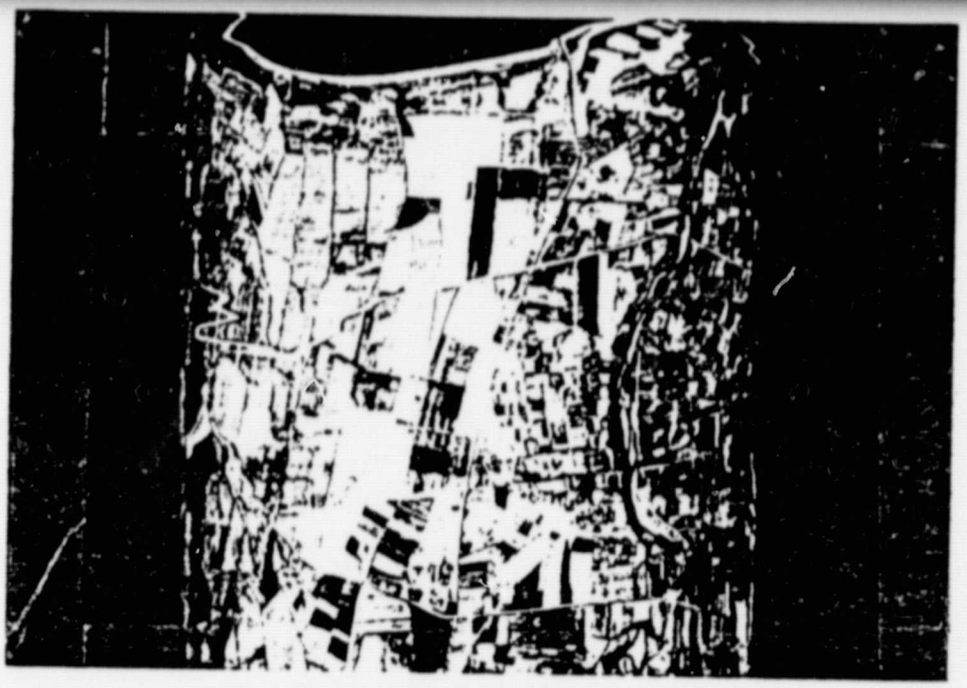

fig. 3.3a

uncorrected

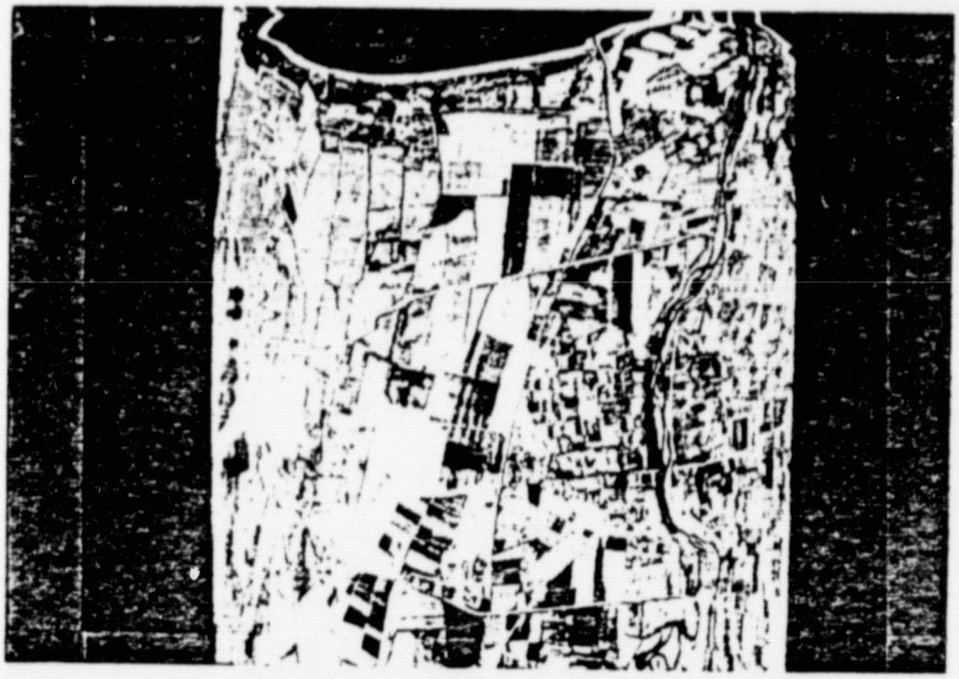

fig. 3.3b

corrected

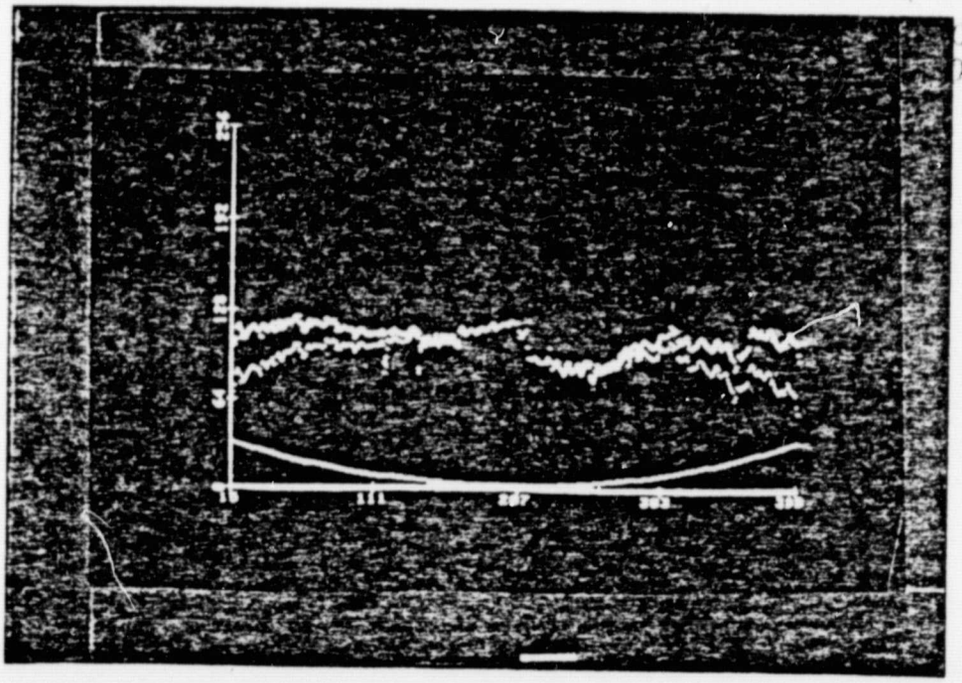

ORIGINAL PAGE IS
OF POOR QUALITY

fig. 3.4

so that multiplying pixel of cooordinates (n_1,n_2) by $(-1)^{n1+n2}$, the requested transform is obtained.

The software in its present form (implemented on IBM 370/158) produces only the spectrum of the image, i.e. being generally the Fourier transform complex

$$F(u,v) = R(u,v) + j\ I(u,v) \qquad (14)$$

the available data are

$$\left|F(u,v)\right| = \left[R^2(u,v) + I^2(u,v)\right]^{1/2} \qquad (15)$$

After the two altitudes images' spectra are obtained, in accordance to (6) the scale change transfer function is carried out by ratioing these spectra. This ratio can be performed either on a point-to-point basis or in an integrated manner.

The first approach is certainly more general, but it is also more subjected to local fluctuations. The integrated approach consists in subdividing the original spectra in a lot of little areas as it is shown in Fig. 3.6.

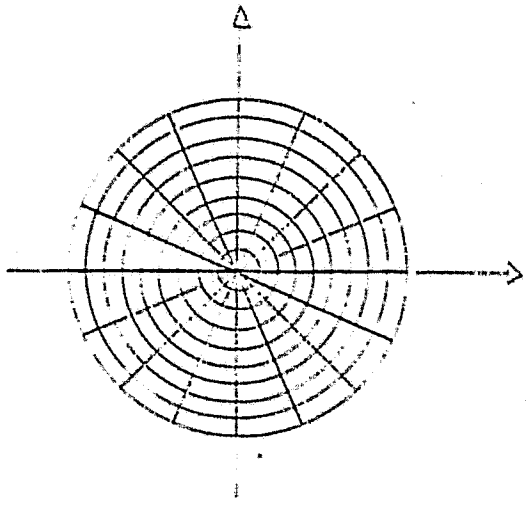

Fig. 3.6

The ratio of partial energies of corresponding regions gives the shape of the G function. On the assumption of circular symmetry of the scale change filter, the regions to be ratioed can simply be the rings.

With respect to the proposal to obtain the scale change function for whatever altitude increase, two cases can occur:

i) If only two altitudes data are available, it is possible to determine only one G function. Supposing the acquisition system used is the same, in order to simulate other altitudes data, the system MTF must be known. It's then necessary to proceed by attempts with the following steps:
   - the hypothesis is made that the system MTF belongs to a certain class of filters;
   - by means of time-scaling and of the model of § 2 the corresponding scale change filter is carried out;
   - a comparison between supposed and true scale change function is realized which gives an answer to how good the choice is.

   When the system MTF is carried out, other altitude increases can be simulated with the method shown in Fig. 3.1.
   Just as an example two filter classes (Lanczos-Cappellini and Butterworth) are presented in Appendix III.

ii) If at least three altitudes data are available, it is possible to determine at least two G functions. Writing these function using the altitude factor as parameter, it is possible to obtain directly the G filter for whatever altitude increment.

3.2. Filtering implementation.

As it is well known, the filtering operation can be performed either in the spatial or in the frequency domain the choice depending on image size and impulse response size. If non-zero impulse response array is large, Fourier domain is more computationally efficient while direct processing is advantageous for large size image. For very large images a block mode filtering technique can be used which processes separately adjacent overlapped blocks [Ref. 10 chapt. 11] .

i) Spatial domain

The two steps of direct convolution and points' decimation can be grouped into a single operation of "convolution by step" on the basis of reduction factor.This permits only integer factor reductions so if it is not case, it is necessary to apply resampling techniques; this is however equivalent to use, as scale change function, a filter different from the projected one.

Attention must be used in handling edges data in order to have a meaningful convolution also along the borders.

ii) Frequency domain

In this case the filtering operation consists in multiplying the image transform by the corresponding samples of scale change filter (multiplication of modules; difference of phases). Now there is no more the restriction to integer reduction factor. While, in fact, in the spatial domain decimation must be used, in frequency domain the same result is obtained cutting away an edge of spectrum data so that, depending on the size of this edge, an arbitrarly reduction can be obtained.

4. COMPARISON TECHNIQUES BETWEEN TRUE AND SIMULATED IMAGES.

After the filtering has been performed some methods must be established to carry out the comparison between simulation output and true image.A pixel-to-pixel comparison must be disregarded because such an approach presupposes a very accurate registration between images. Also taking into account the phase factor and on the hyphotesis that images don't have any geometrical distorsions, the registration averaged error for N reduction factor is 1/2N of the low resolution pixel dimension.It follows that for small reductions (just like aircraft data simulations) this error would be rather high.

Instead of local techniques it is then convenient to use the image global informations. These techniques can be summarized as follows:

i) image analysis in the space domain
   - histograms comparison
   - entropy computation for the two images. Referring to [Ref. 11] it is possible to define the entropy of an image as

$$S = -\sum_{i=1}^{N} p_i \log_2 p_i \qquad (16)$$

where with p_i has been denoted the i^{th} level probability (it is interesting to note the introduction, in the same paper, of a specific entropy, i.e. a value indipendent of image area).
This method permits to realize a comparison of two images simply by the comparison of two numbers.

ii) Image analysis in the frequency domain.
- computation of spectra correlation.
  In the transform domain the problems arising from a point-to-point comparison are smaller than in the space domain. Here, in fact, the registration of two spectra gives no problem unless the original lines of flight were not perfectly parallel; in such a case the true and simulated image spectra are slightly rotated one in respect to the other. If this is not the case, it is then possible to estimate the similarity between images by means of a measure of correlation of spectra. Anyone of known fidelity function [Ref. 12, vol. 3.1, 1.4.2.3.] can be used; the sum of absolute values of differences will be used in the following
- Spectra energy computation in corresponding regions.
  If an accurate registration between spectra is not possible, an averaging technique must be used. Remembering that the energy of a signal is the square of its spectrum, the total energy of the Fourier transform of each image is calculated adding the energy at each point (u,v)

$$E_T = \sum_{u=0}^{N-1} \sum_{v=0}^{N-1} E(u,v) \qquad (17)$$

with u,v=0,...,N-1.

Calculating then the energy enclosed in circles or circular rings with origin at the center of the frequency domain, it is possible to compare the corresponding energy percents β of the two spectra.
This is obtained by calculating

$$\beta = 100 \left[\sum_{u} \sum_{v} E(u,v)/E_T \right] \qquad (18)$$

where the summation indices range over the samples lying inside the circles or the rings.

Another averaging technique makes use of circular sectors. If, however, a rotation between spectra is present, the circles/rings method must be preferred.

5. APPLICATION EXAMPLE

Just as an example of the use of techniques seen in previous paragraphs, a simulation of an aircraft day image in the infrared channel is now examined. The data collection was made during the 1978 joint flight experiment on test site Sibari by means of a Bendix MSS. During this compaign data were detected at different aircraft altitudes (500, 1000, 1800, 3000m) but as a first attempt only 500 → 1000m simulation had been put into practice.

The region considered (seen at 500m) is reported in Fig. 5.1.

According to the procedure described in § 3.1, the following steps have been implemented:

- correction of 500m and 1000m original images. Since the Bendix PSF isn't known, the only corrections have been made concern the optical depth increase for scan angle and the panoramic effect. About the former, the correction has been at first calculated referring to an almost uniform region and has then been applied to the whole 500m image. Fig. 5.2 shows the profiles (averaged on a number of lines) of the uncorrected and corrected image. The same procedure has been repeated for 1000m image. The panoramic effect has been corrected resampling data (with a cubic polynomial) in the scanning direction. The algorithm has produced, using 803 input samples, 1256 output pixels. A visual effect of this correction is shown in Fig. 5.3 where uncorrected image (Fig. 5.3a) is compared with the corresponding panoramic effect corrected image (Fig. 5.3b). The two images are left-aligned (corresponding to flight line) so that pixels' number increase becomes evident (a symmetric effect on the other side).

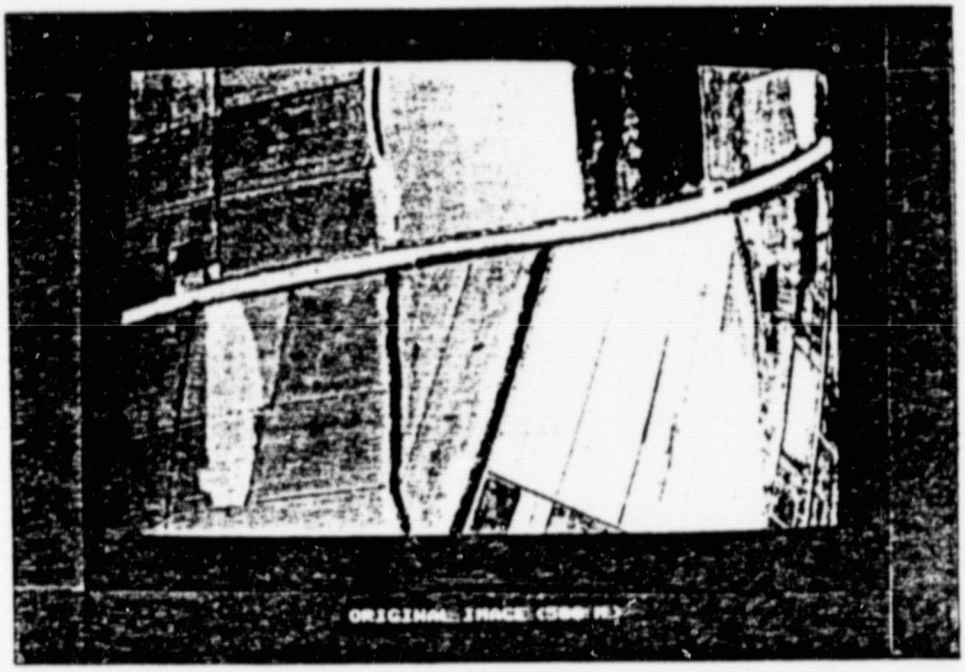

Fig. 5.1

ORIGINAL PAGE IS
OF POOR QUALITY

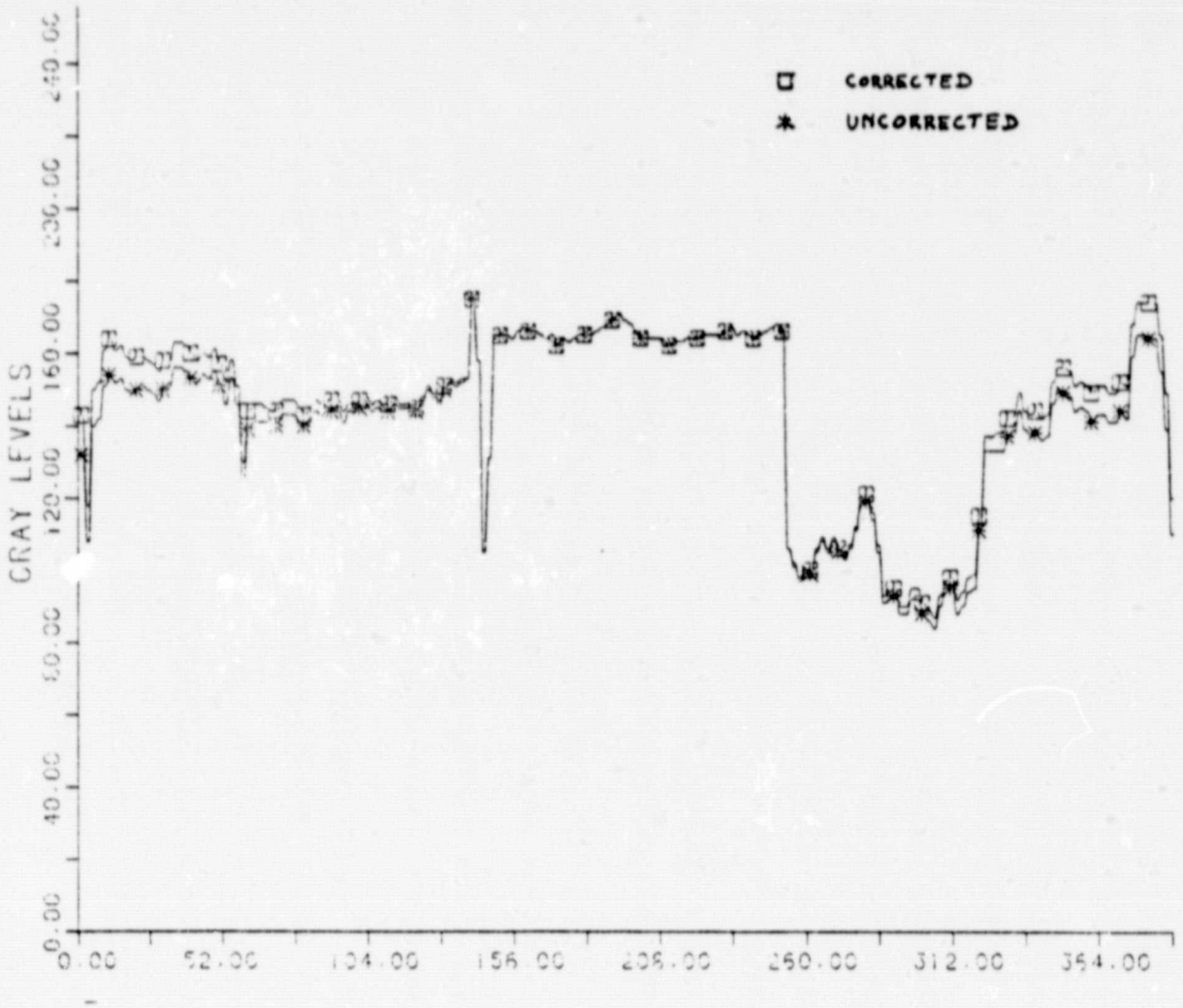

Fig. 5.2

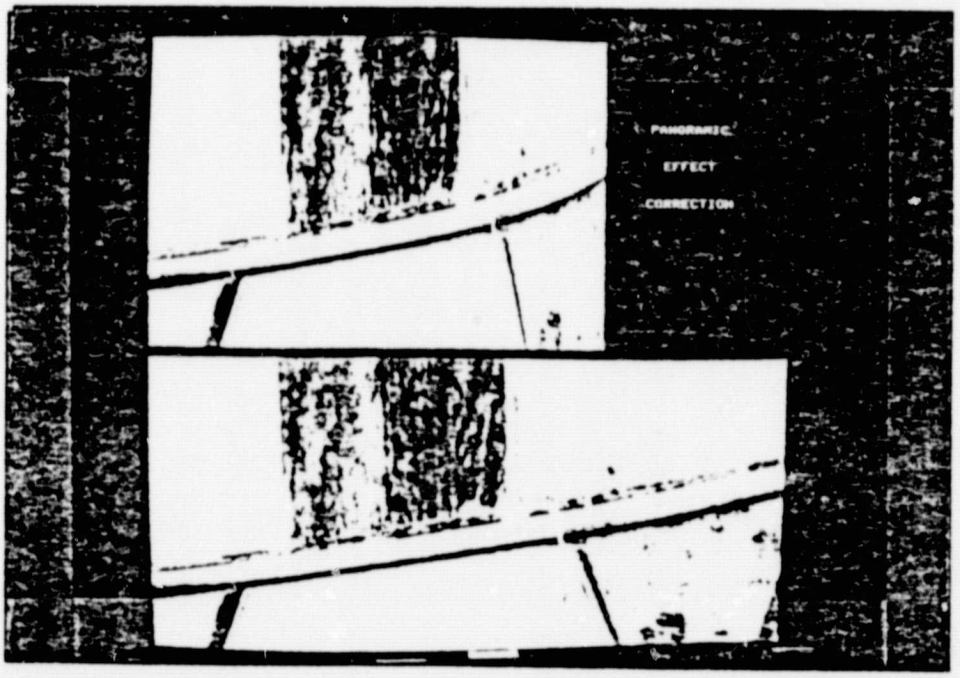

(a)

(b)

Fig. 5.3

- Choice of test area.
  The simulation procedure is performed on a segment 512x512 pixels dimensioned.

  In the whole region of Fig. 5.1, the area shown in Fig. 5.4 has been chosen because of the presence of spatial structures. For homogeneous area, in fact, the scaling-up output is independent from used PSF so this case isn't meaningful for test.

  The scale change procedure should give an output similar as much as is possible to the true 1000m image (reported in Fig. 5.5).

- Fourier spectra computation.
  The developed software in its present form, neglects the phase information; besides since the dynamic range of transform is very large and in order to display it in image form on I^2S imaging system, it's necessary to compress the coefficient values in byte format. The whole spectrum range is then linearly subdivided into 256 levels.
  Images of Fig. 5.4 and 5.5 are used as input to Fourier spectrum computation program. The resulting outputs are respectively reported in Fig. 5.6 and 5.7. For visual reasons they report the quantity $1+\log_{10}|H|$.

  As it has been stated in § 2.2, the spacing between frequency samples is the same, i.e., $\Delta u = 1/T_0$ where $T_0 = N\Delta x$. In this case for 500m image spectrum $\Delta x = 1.25$m, $N=512$ while for 1000m image spectrum, $\Delta x = 2.5$m, $N=256$. It follows that the frequency domain dimensions are (see also [Ref. 8 pg. 78])

$$512\ \Delta u = \frac{1}{1.25}$$

$$256\ \Delta u = \frac{1}{2.5}$$

The maximum revealable frequencies are

$$0.5\ \frac{1}{1.25} = 0.4 \text{ cycles/m}$$

$$0.5\ \frac{1}{2.5} = 0.2 \text{ cycles/m}$$

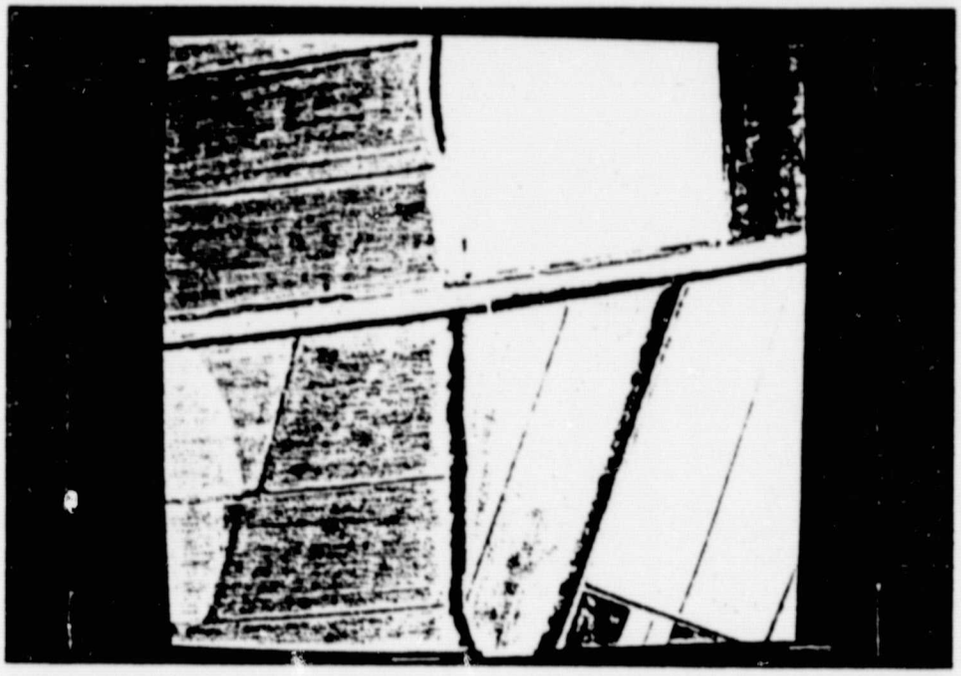

fig. 5.4

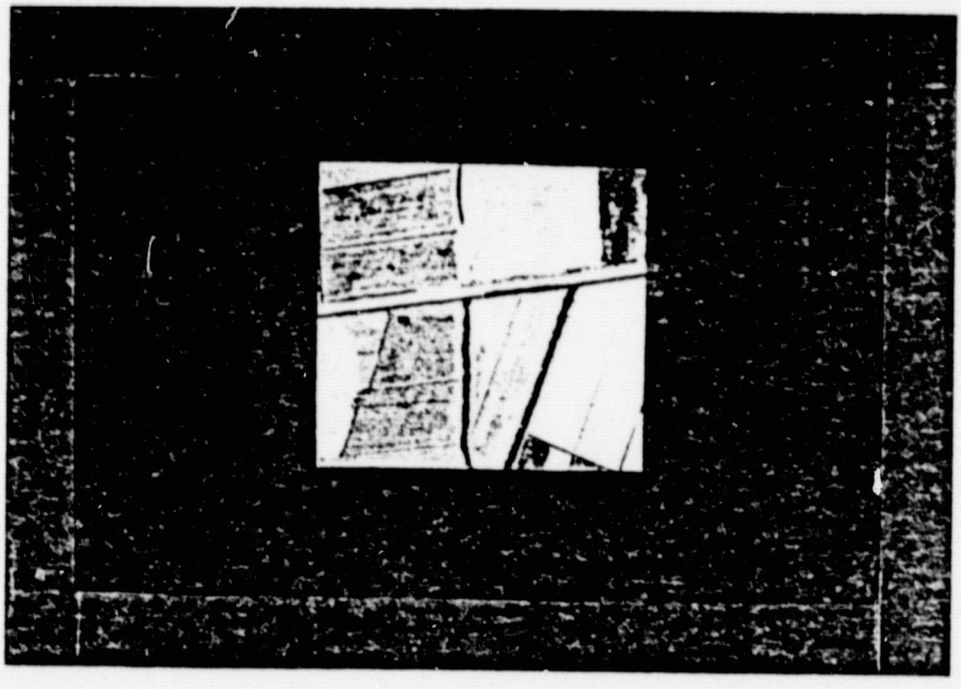

fig. 5.5

ORIGINAL PAGE IS
OF POOR QUALITY

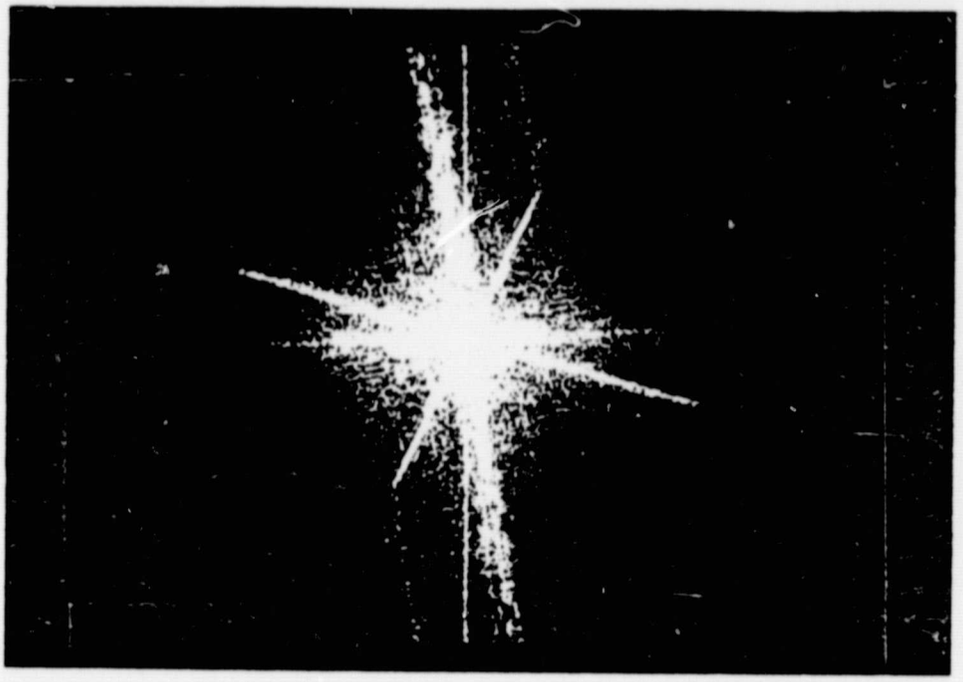

fig. 5.6

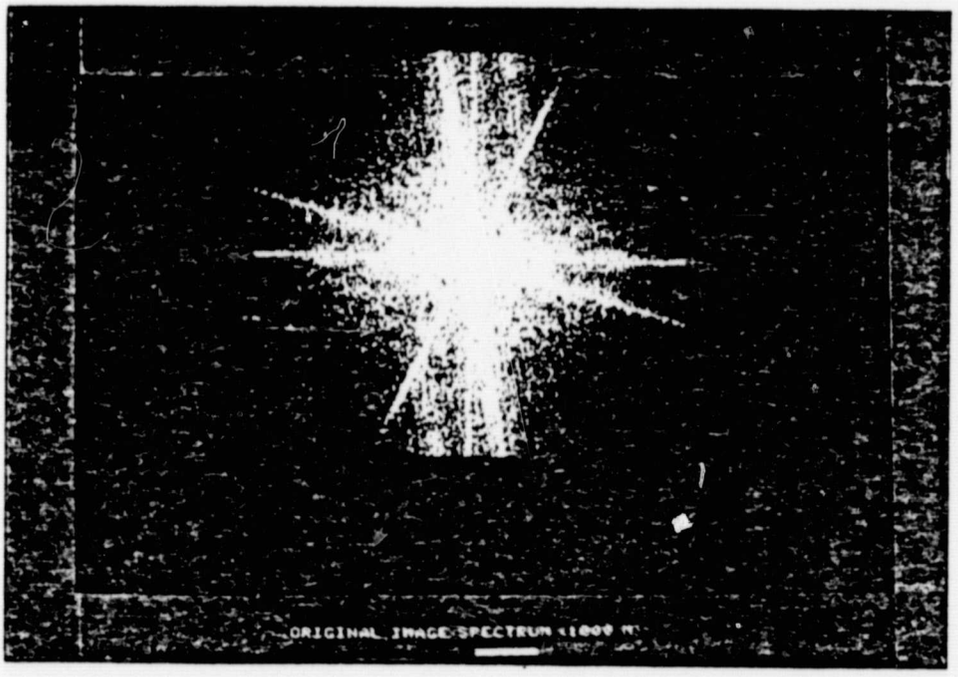

fig. 5.7

- Ratio of spectra.
  As it has been stated in § 4, the ratio of spectra can be realized either in an integral mode or in a point-to-point mode.

  An example of the former approach is reported in Fig. 5.8 which shows one of the rings the Fourier plane can be subdivided in. The technique used is, however, the local ratio one; the (normalized) output is in Fig. 5.9. The presence of structures in the spectrum can be ascribed to a little non-compensated rotation between the two original images spectra.

- Determination of an analytical scaling-up filter.
  As it has been stated in §3.1, it is convenient to determine which class of analytical filters fits the true scaling-up filter.
  In this case it has been seen that the ratio of a Butterworth filter of order 3 and cut-off frequency 120 with its scaled version produces a G' function which resembles the shape of the G filter (Fig. 5.10). According to the model, the acquisition chain object-data at 500m altitude can be then represented by a MTF shaped just like a Butterworth filter (f_{cut}=120; order 3) so the corresponding G filter for whichever other altitude increase can be easily carried out.

- Scaling-up simulation.
  The image filtering has been performed in the space domain. Frequency domain filtering requests, in fact, the multiplication of the spectrum by the filter. Since both have a quantization error and because the result must be re-quantized and antitransformed, referring to the present software, this approach would be meaningless (for a good treatment of quantization techniques see [Ref. 9 chapt. 7]). The two dimensional spatial array obtained from G' antitrasformation has been convolved with the image of Fig. 5.4 and the result has been compared with Fig.5.5.

- True and simulated images comparison.
  Referring to the techniques exposed in § 4, the histograms of the whole images have been obtained (Fig. 5.11). As it is evident, there is no similarity between them. This effect becomes, however less evident if the histograms regarding a region symmetrical respect to the flight lines are considered (Fig. 5.12). The difference still remaining between them can be further reduced by means of a linear transformation. Calling, in fact, $x_1, M_1, S_1 (x_2, M_2, S_2)$

respectively the gray level, the average value and the variance of the simulated (original) image, a new image has been obtained with gray values x_1' carried out by means of the relation

$$x_1' = ax_1 + b$$

where

$$a = \frac{S_1}{S_2}$$

$$b = M_2 - aM_1$$

Fig. 5.13 shows the comparison between the original and the new simulated image histograms.

The hypothesis can be made that this linear transformation accounts for atmosphere increase with altitude.

When the transformation has been applied to the whole image no improvement has been obtained.

Two possible causes are suggested to justify this result:
- along-flight direction pixels correlation (the correction of panoramic effect has been realized, in fact only in the scanning direction without considering the enlargement of the pixel also in the flight direction)
- shift-variant components present in the Bendix MSS PSF.

As a further comparison method, the simulated image (complete) Fourier spectrum has been compared with the original one. From a visual inspection the filtering output is too lacking in high frequencies in respect to the true 1000m image. i.e. the filter used has been revealed as the incorrect one.

As an experiment all the operations have been repeated with the Lanczos-Cappellini filter with parameters (N=16; α=0.25; m=15) . Histograms and spectra reveal however, no meaningful improvement respect to the first attempt.

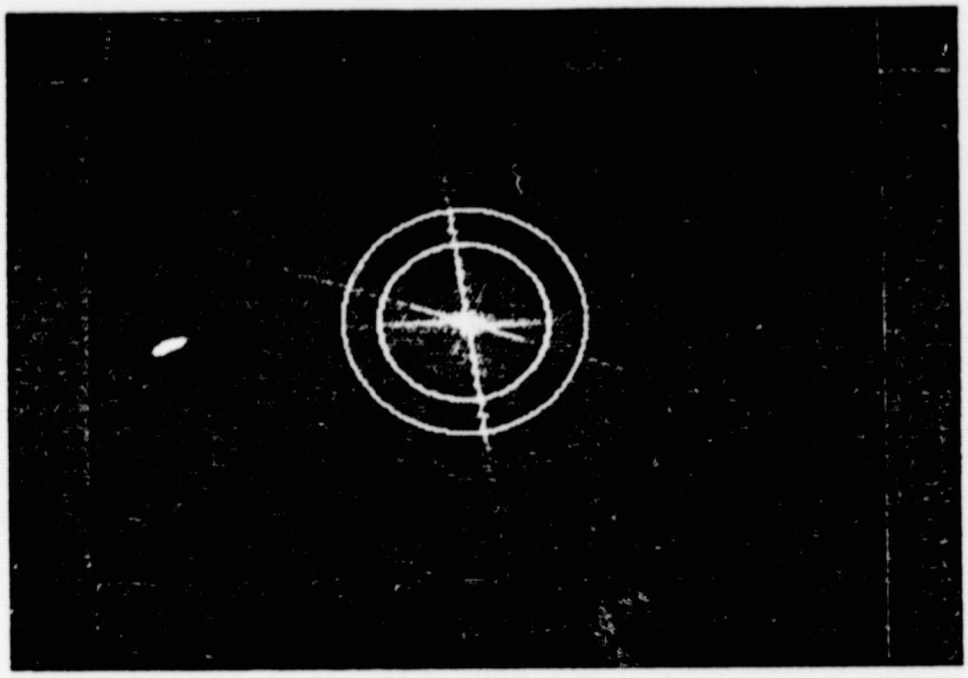

fig. 5.8

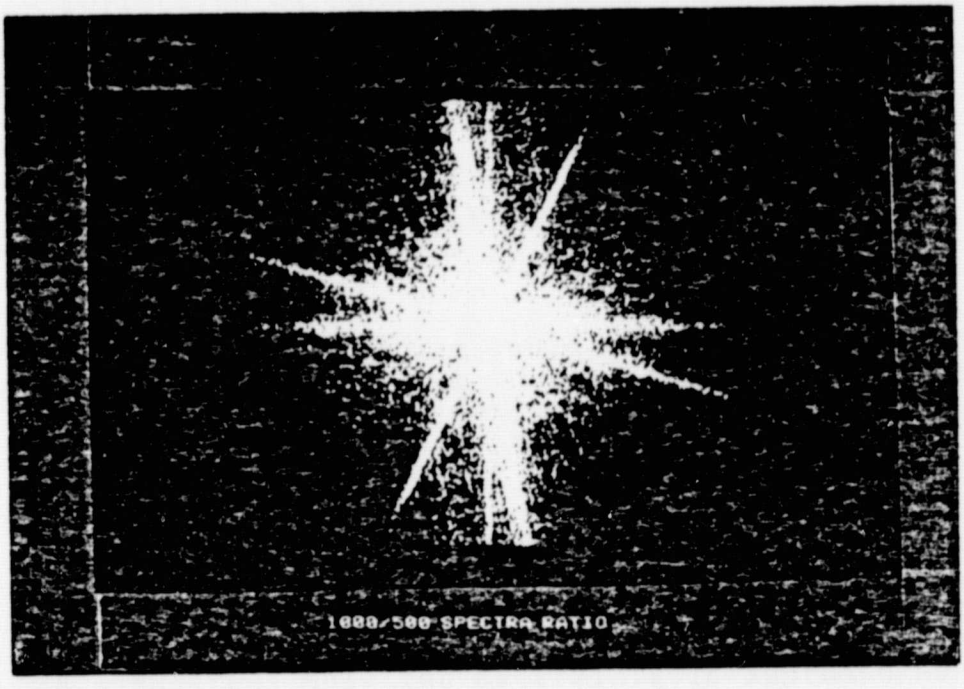

fig. 5.9

ORIGINAL PAGE IS
OF POOR QUALITY

6. CONCLUSIONS

The most important results arising from this work can be summarized as follows:
- singling out of main problems which must be faced in scaling-up simulations
- determination of a simulation method
- software implementation of the method.

The lack of informations on used acquisition system hasn't permitted the realization of an exhaustive test of the proposed scaling-up methodology.

Even more so HCMM images haven't been not simulated also because of the difficulty of registering the few pixels coming from test-site data with a whole HCMM scene.

Further developments can be however proposed to improve the method. They can be so summarized as follows:
- utilization of atmospheric models to take into account the increase of the atmospheric layer
- correction of panoramic effect also in the flight direction
- better registration between the two altitudes starting images (if a rotation must be performed, it is convenient to subdivide it into two opposite half-rotations; this avoids the resampling affects in different manners the two images)
- introduction of the phase term in the Fourier transform computation and usage of non-integer values for the transform itself.

Beside these,the module could be developed to carry out the scale change filter in a parametric form (see § 3.1) using three altitudes data; this avoids, in fact, the step of the determination of instrument MTF.

Many aspects of the proposed empiric approach make useful the approach itself only for the simulation of different altitudes data detected by the same acquisition system. If, on the contrary, images detected by different systems must be simulated, only the deterministic approach can be used. The problem must then to be faced to know with a sufficient approximation degree the MTF of the acquisition system and after to apply the method of pg. 12 .

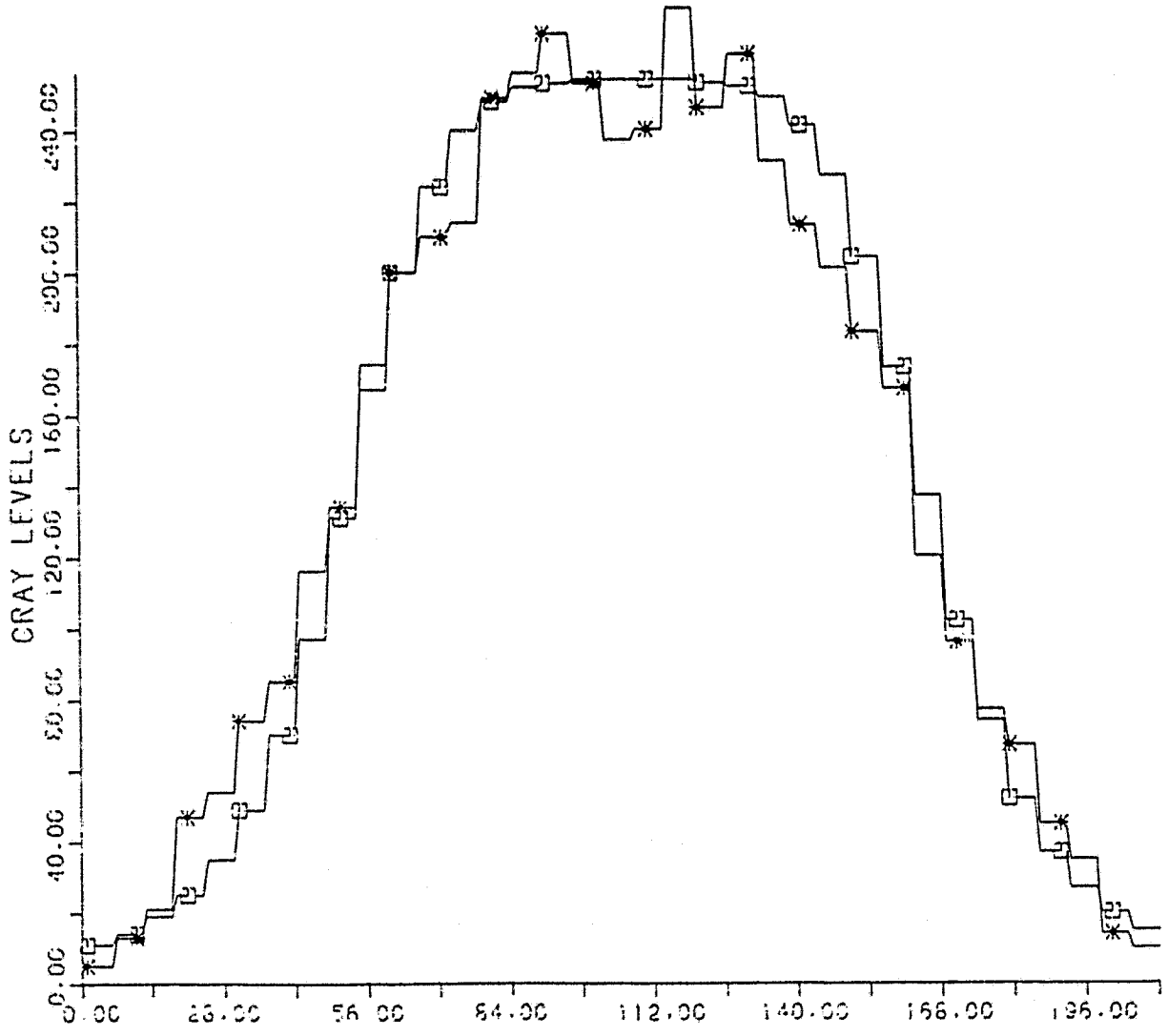

□ = Butterworth filter

* = ratio filter

Fig. 5.10

500 m. image histogram

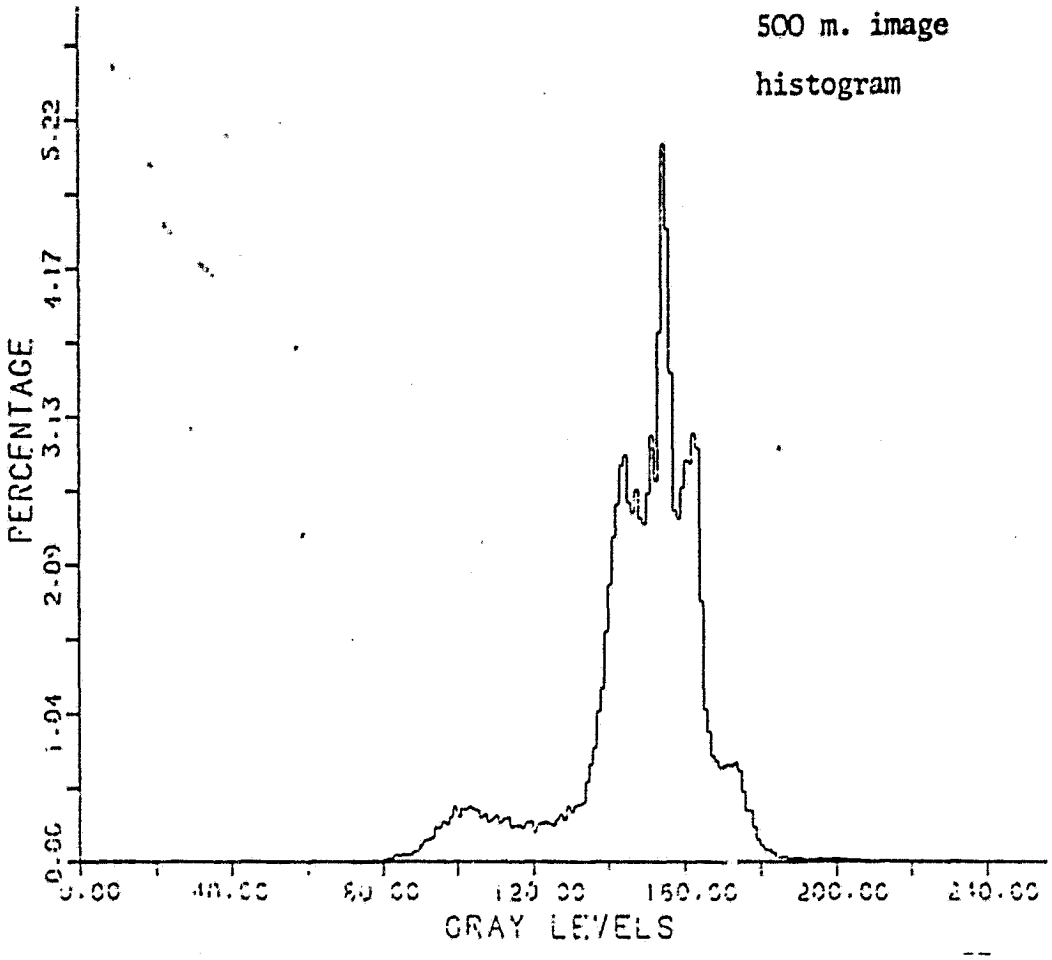

1000 m. image histogram

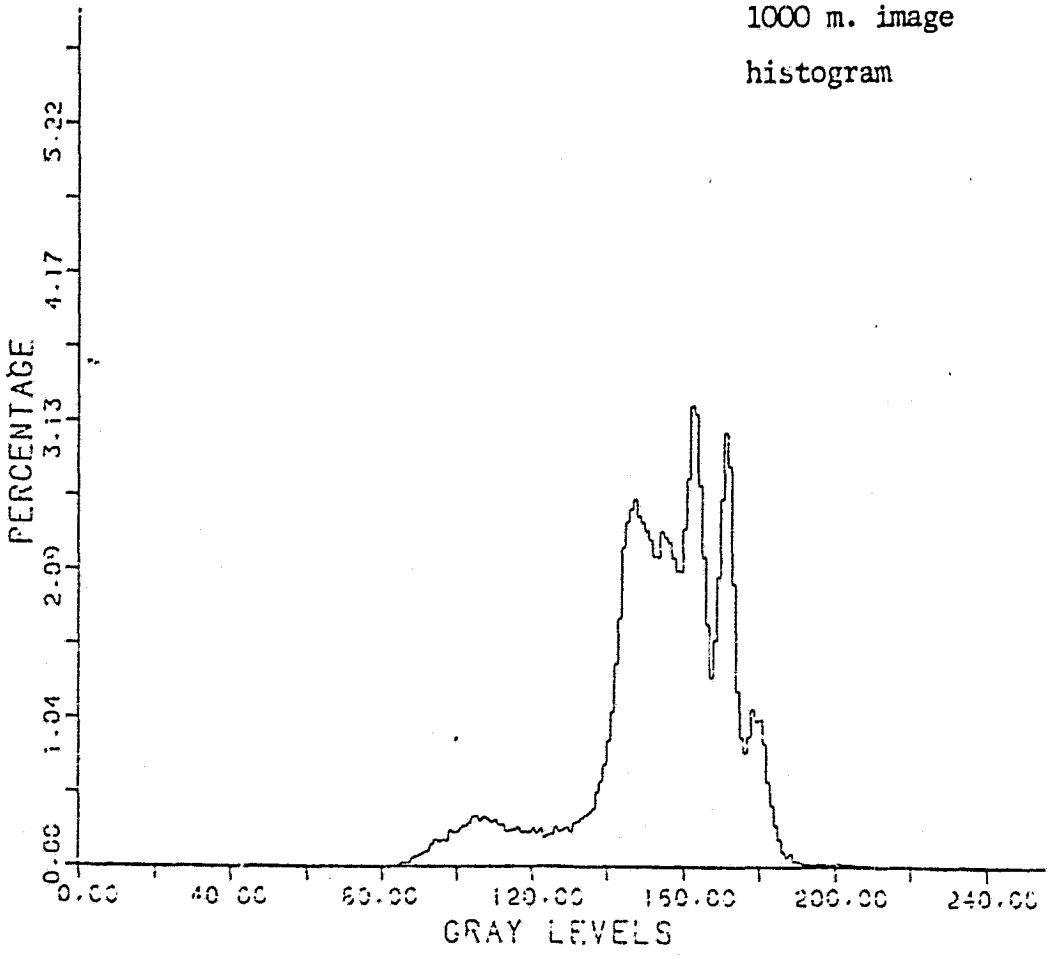

fig. 5.11

500 m. image
histogram

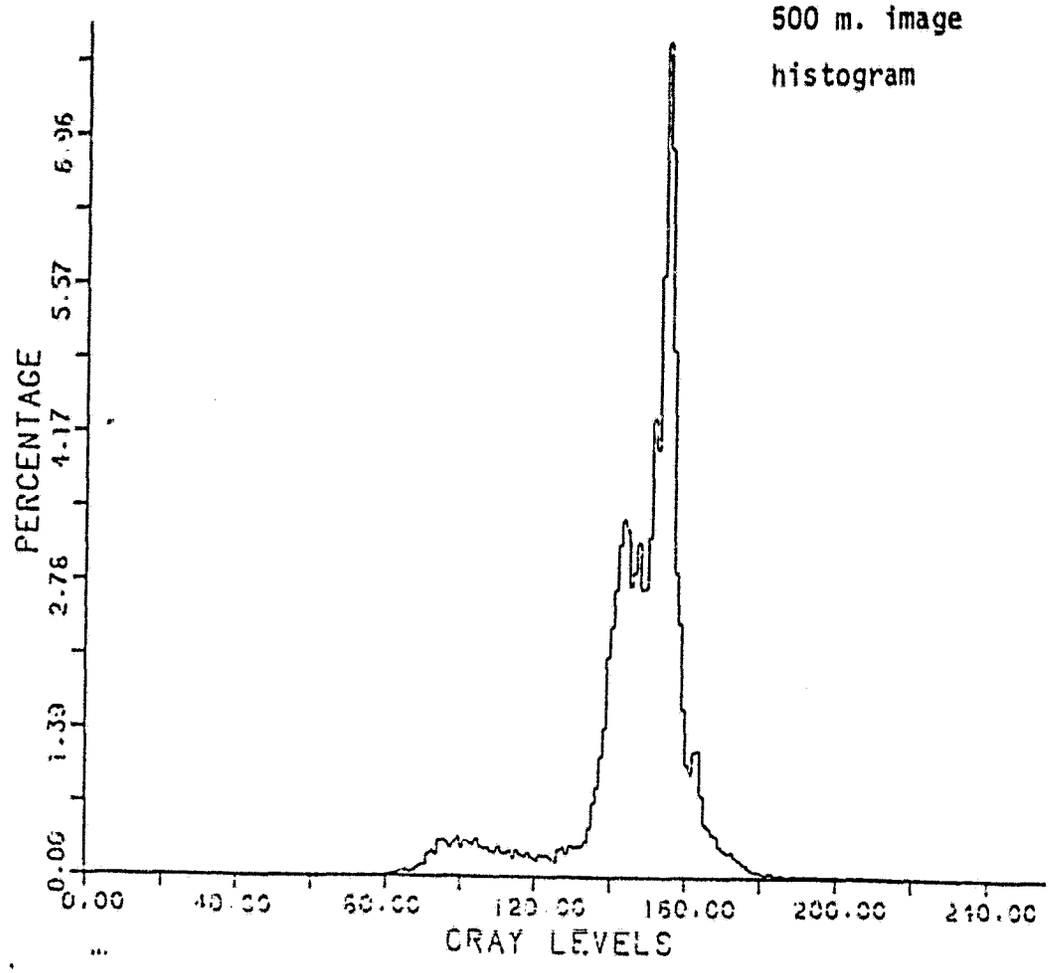

1000 m. image
histogram

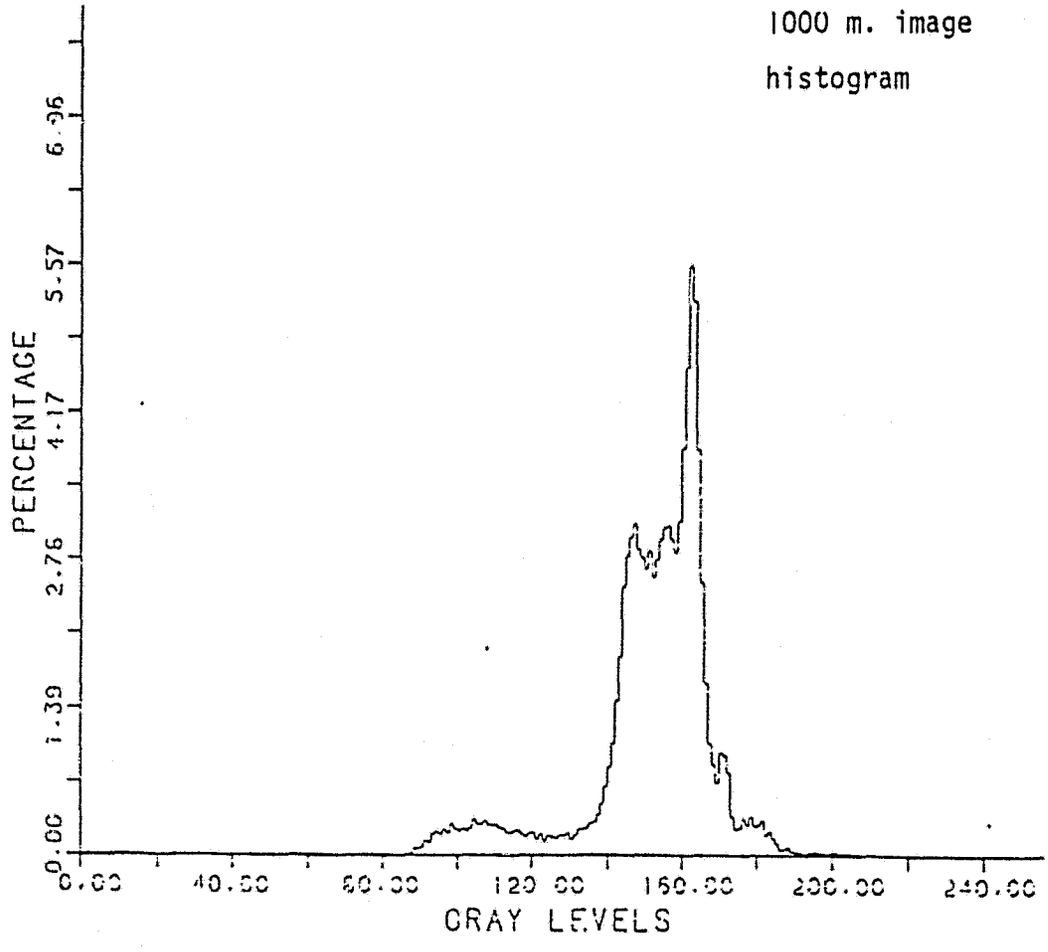

fig. 5.12

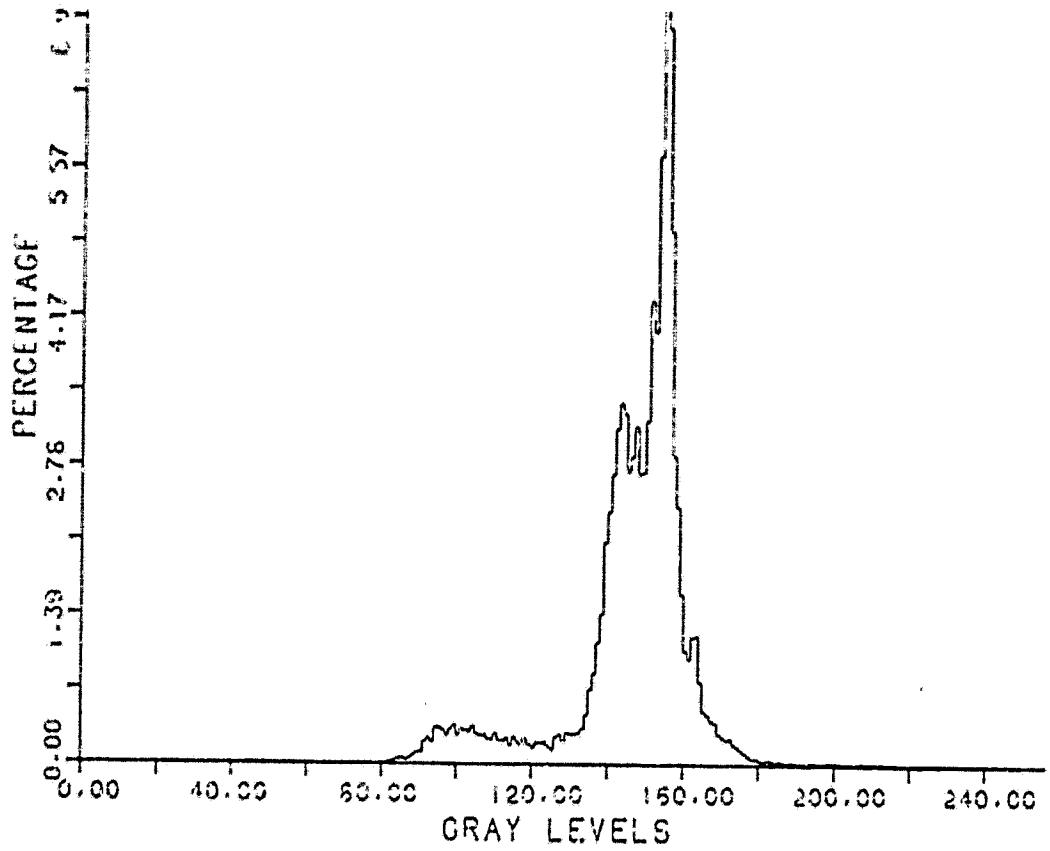

Fig. 5.13 (a)

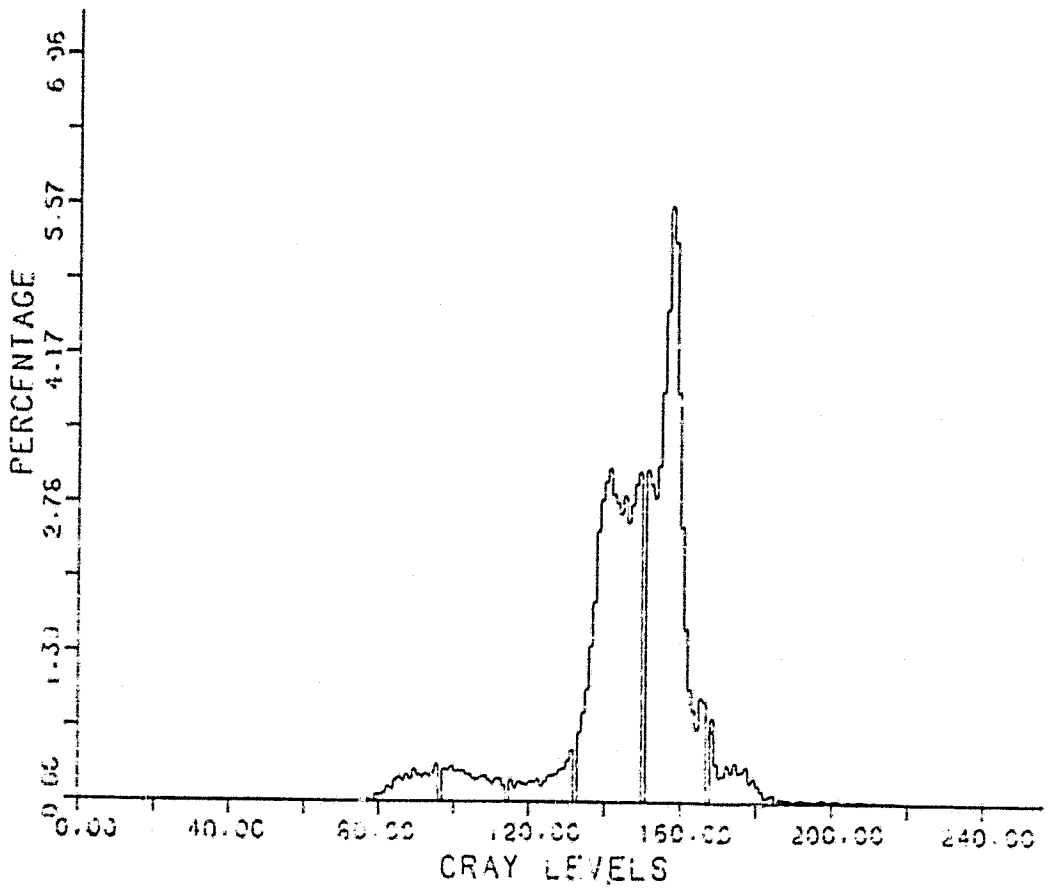

Fig. 5.13 (b)

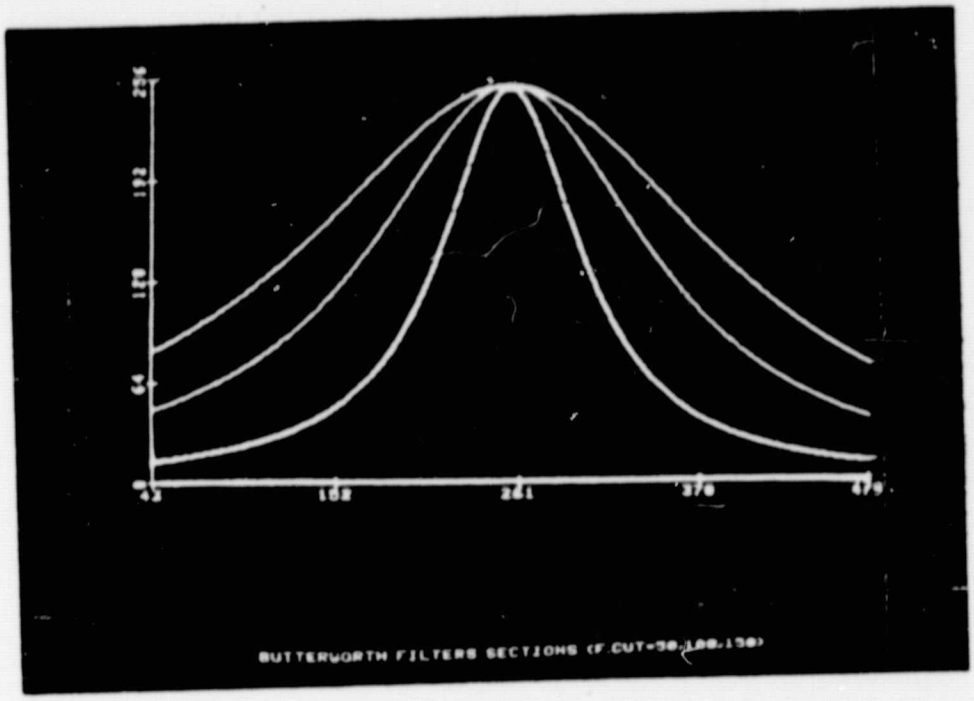

Fig. A.III.4

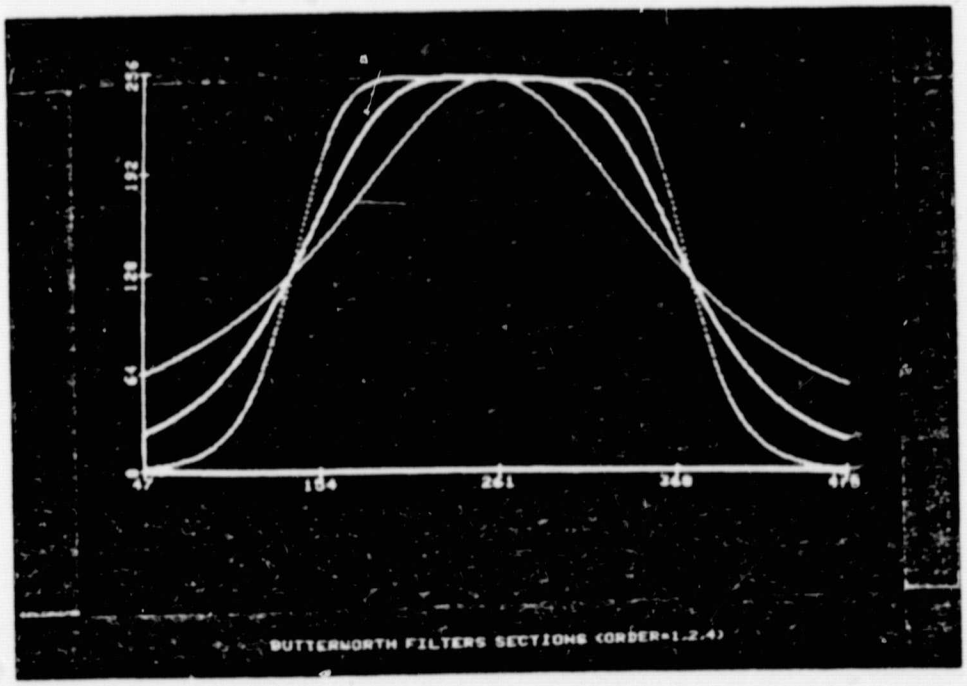

Fig. A.III.5

ORIGINAL PAGE IS
OF POOR QUALITY

REFERENCES

1 - Mundie and others
System design considerations for advanced scanners for earth resource applications
Proc. IEEE, vol. 63, n. 1, jan. 1975, pg. 95.

2 - Rosenfeld, Kak
Digital picture processing
Academic Press, 1976.

3 - Brigham
The fast Fourier transform
Prentice-Hall, Inc.

4 - Liu, Gallangher
Optimum Fourier transform division with magnitude constraint
Journ. Opt. Soc. Am., vol. 64, n.9, sept.1974, pg.1227.

5 - Turner, Malila, Nalepka
Influence of the atmosphere on the remotely sensed data
Proc. Soc. Ph. Opt. Instrum. Eng. vol. 51, august 1974, pg. 101.

6 - Potter
Haze and sun angle effects on automatic classification of satellite-data and correction
Proc. Soc. Ph. Opt. Instrum. Eng. vol. 51, august 1974, pg. 73.

7 - Cappellini and others
Digital filters and their applications
Academic Press, 1978.

8 - Gonzales, Wintz:
Digital image processing
Addison-Wesley, 1977.

9 - Andrews
Computer techniques in image processing
Academic Press, 1970.

10 - Pratt
Digital image processing
Pre-pubblication copy.

11 - Lechi
Le carte tematiche e le loro risoluzioni
Proc. II Site Conference Varenna, sept. 1979 (not yet published).

12 - Csata - Esoc contract
An image processing support software (IPSS)
contr. n. 2800/76/D/IM/SC, Bari, april 1978.

13 - The optical industry and systems directory
Encyclopedia
1979, vol. 2.

14 - Kidd, Wolfe
Performance modeling of earth resources remote sensors
IBM Jour. Research and Development, january 1976, pg. 29.

15 - O'Neill
Transfer function for an annular aperture
Jour. Opt. Soc. vol. 46, n. 4, april 1956, pg. 285.

16 - Papoulis
System and transforms with applications in optics
Mc Graw-Hill, 1968.

17 - Stokseth
Properties of a defocused optical system
Jour. Opt. Soc. Am., vol. 59, n. 10, october 1969, pg. 1314.

18 - Lerman, Shannon
Two-dimensional image prediction and enhancement
Proceeding SPIE, vol. 10, 1967.

19 - Barbe
Imaging devices using the charge-coupled concept
Proc. IEEE, vol. 63, n. 1, January 1975, pg. 38.

20 - Hufnagel, Stanley
Modulation transfer function associated with image transmission through turbulent media
Jour. Opt. Soc. Am., vol. 54, 1964, pg. 52.

21 - Aboutalib, Silverman
Restoration of ratio-degraded images
IEEE Trans. Circuits Syst. CAS-22, 1975, pg. 278.

22 - Proceedings CALTECH/JPL conference on image processing, Technology, data sources and software for commercial and scientific applications
1976.

23 - Istituto elettrotecnica, Genova-Esoc contract
Study on the use of the fast Fourier transform in spectral analysis
Contr. n. 486/73 Esa (Esro) cr-468, Genova, sept. 1975.

24 - Kulhanek
Introduction to digital filtering in geophysics
Elsevier, 1976.

25 - Huang
Picture processing and digital filtering
Springer-Verlag 1975.

APPENDIX I

SURVEY ON POINT SPREAD FUNCTION (PSF) AND MODULATION TRANSFER FUNCTION (MTF).

The image formation process by means of an imaging system (see Fig. A.I.1).

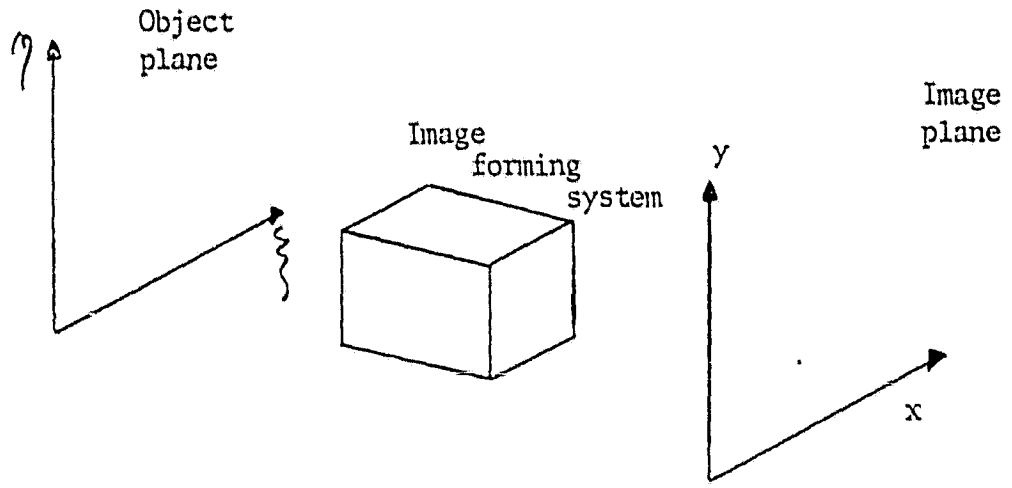

Fig. A.I.1

involves a redistribution of radiance coming from the object. Generally this redistribution must take into account the radiance in the whole image plane, but if the process is linear, then the image of an extended source is obtainable by superimposing the images of single object points. The degradation introduced by imaging system is then represented by the spatial distribution on image plane of the single source point and it is mathematically expressed by the point spread function (PSF). Denoting with $o(x,y)$ and $i(x,y)$ respectively the object and image functions and with $h(x,y)$ the PSF, the linear imaging process is then represented by

$$i(x,y) = \int_{-\infty}^{+\infty}\int_{-\infty}^{+\infty} o(\xi,\eta)\, h(x,y;\xi,\eta)\, d\xi d\eta \qquad \text{(A.I.1)}$$

The four indices for impulse response denote that its shape can change depending on input and output coordinates. If, on the contrary, each point in the object plane contributes to the image point with a "strenght" depending only on its relative position, the system is said to have a shift-invariant point spread function (SIPSF). In this case the (A.I.1) becomes the superposition integral

$$i(x,y) = \int_{-\infty}^{+\infty}\int_{-\infty}^{+\infty} o(\xi,\eta)\, h(x-\xi,y-\eta)\, d\xi d\eta \qquad \text{(A.I.2)}$$

This expression is nothing but the convolution of $o(x,y)$ with $h(x,y)$, denoted also with

$$i(x,y) = o(x,y) \otimes\otimes h(x,y) \qquad \text{(A.I.3)}$$

If the Fourier domain is now considered (obviously with spatial frequencies), it is possible to associate each spatial function with its Fourier transform. These new functions are complex ones and so each of them can be written in the form

$$R(u,v) = P(u,v) + jQ(u,v) = M(u,v)\, e^{j\phi(u,v)} \qquad \text{(A.I.4)}$$

Starting from the Fourier convolution relationship (i.e. the corrispondence between convolution and multiplication in spatial and frequency domains as it is shown in Fig. A.I.2)

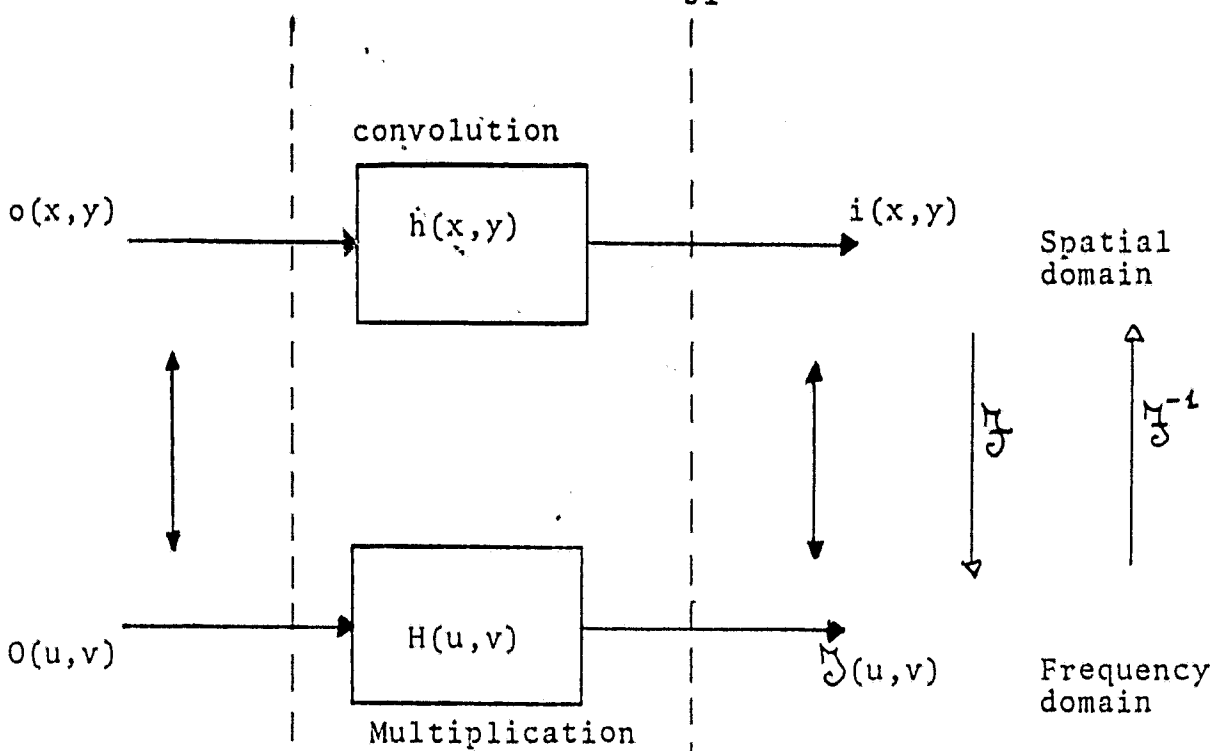

Fig. A.I.2

the expression (A.I.3) becomes

$$I(u,v) = O(u,v)\, H(u,v) \qquad \text{(A.I.5)}$$

Considering the PSF transform, it is usually known as Optical Transfer Function (OTF). In particular its amplitude response is called Modulation Transfer Function (MTF) while the phase response is the Phase Transfer Function (PTF).

It must be noted that in the practice phase variations are often disregarded and so the imaging system degradations are represented either by PSF in the spatial domain or by MTF (referred to in the text by means of capital letters) in frequency domain. This pair of functions is usually called Fourier pair and it is sufficient to identify the imaging system.

A useful characteristic of MTF is its "multiplicative property", i.e. if an imaging system is set up with more cascaded devices, the global MTF is carried out by the product os single components' MTFs.

It must be underlined that the definition of an univocal MTF is possible only for SIPSF.

If on the contrary shift variant PSF (SVPSF) are involved, Fourier techniques are no longer applicable and the use of very complex mathematical techniques is required [Ref. 25 pg. 24, pg. 52] .

APPENDIX II

SURVEY OF PRINCIPAL DEGRADATIONS OF AN ACQUISITION SYSTEM.

Referring to a typical remote sensor configuration, it can be represented as in fig. A.II.1

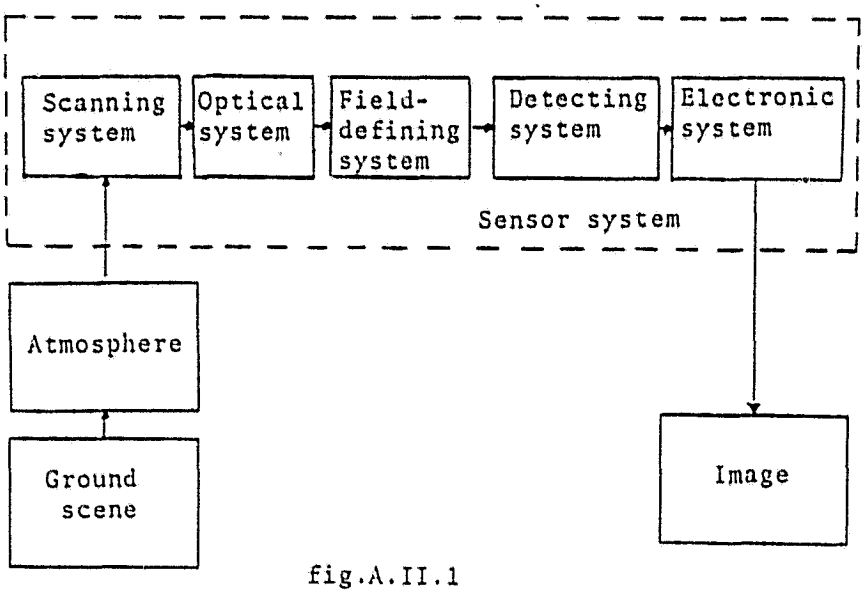

fig.A.II.1

If its performance is to be evaluated, two approaches are possible:

- the direct method, i.e. the Modulation Transfer Function of sensor system is determined by a variety of laboratory measuring techniques [ref. 13 pg. e-297]
- the indirect method i.e. a model of the system is constructed For this approach the mathematical model of each component of sensor system must be known and then the global MTF is carried out by making use of multiplicative property for MTFs of cascading system elements [ref. 13, pg. e-291] .

For the indirect method to give meaningful results, it is necessary to know all the degradation sources of the system and their mathematical formulation.

Examining at first the sensor system, its single components can be considered:

- scanning system

Quite apart from the scanning mechanism used (rotating or oscillating mirror) there are often variations in the angular rate of the mirror which distort the image changing its frequency content.

It must also be remembered that the ground is scanned an angular displacement to either side of the nadir. This gives a change of effective pixel's dimensions. A good account of this problem can be found in [ref.14 pg. 33] . It can be summarized here saying that in considering only frequencies in the scan direction (fy=0), the corresponding transfer function is

$$T_{ap}(f_x) = \text{sinc}\,(D_x f_x \sec\vartheta)\ \text{sinc}\,(D_y f_y \tan\vartheta \sec\vartheta)$$

where $D_{x,y} = W_{x,y}\ H/F$

$W_{x,y}$ = detector dimensions

H = platform altitude

F = focal lenght

ϑ = off-nadir angle

In a general manner, called $f_a = H\left[f_x^2 \sec^4\vartheta + f_y^2 \sec^2\vartheta \right]$ a generical spatial frequency measured in cycles/radian, it is possible to write

$$T_{ap}(f_a) = \text{sinc}\,(f_a\ \delta_x\ \cos\vartheta)\ \text{sinc}\,(f_a\ \delta_y\ \sin\vartheta)$$

where $\delta_{x,y}$ are the angular dimensions of IFOV

- optical system

Since the optical system has finite dimensions, the

diffraction phenomenon is unavoidable. If the use conditions allow the assumption that the system is aberration free and if the aperture is circular shaped, the PSF has the usual Airy diffraction pattern with the central disk (i.e. limited by the first obscure ring) containing the 84% of global radiance.

If the resolution properties are expressed as transfer function then [ref. 14]

$$T_{optics}(f_a) = \begin{cases} \frac{2}{\pi}\left[\arccos a - a\,(1-a^2)^{1/2}\right] & 0 \leq a \leq 1 \\ 0 & a \geq 1 \end{cases}$$

where $a = f_a\,\lambda/D$

D = lens diameter

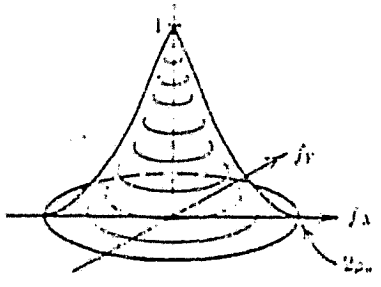

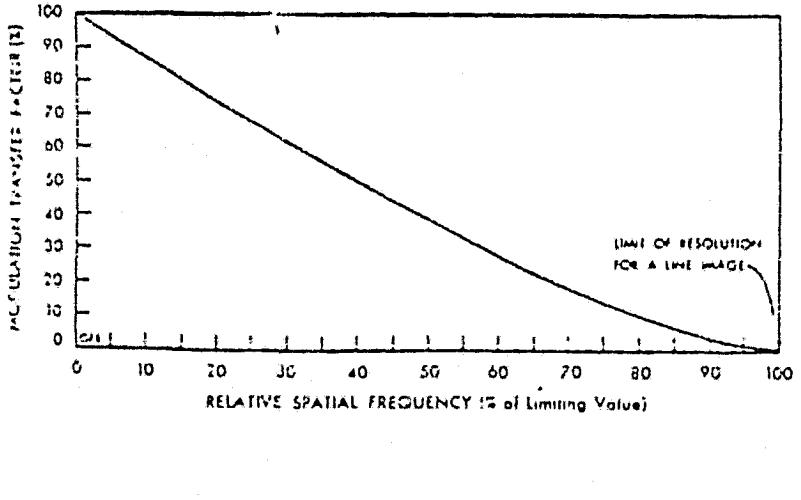

It must however be remembered that the usual scanner configuration has the primary mirror partially obscured by the secondary mirror and this gives an energy redistribution in the diffraction figure. The theory of this can be found in [ref. 15; ref. 16, pg. 336] ; to have, however, an idea of the behaviour, if ρ and $\eta\rho$ are respectively the external and internal radii of the aperture, fig. A.II.2 shows the dependence of MTF from η parameter. From this it is evident that the introduction of a central obscuration reduces the responce at lower frequencies while it improves at higher frequencies.

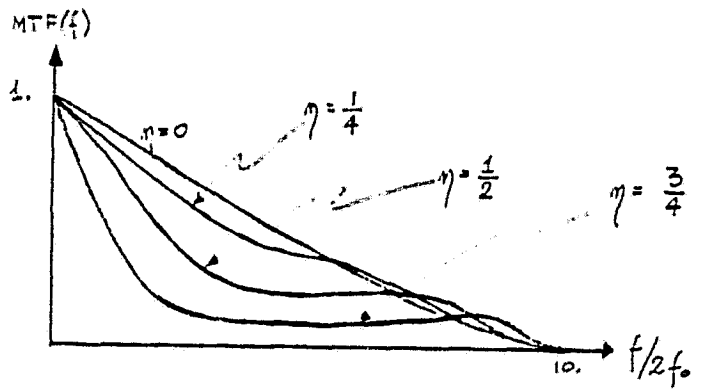

fig. A.II.2

Up until now aberrations have been neglected; this is however not quite correct because in the components of photoelectronic imaging system they are the major degradation sources.

Referring to aberration as a phase variation, it is possible to demonstrate that it produces at each frequency a lowering of transfer function. In a general manner, in the phase variations expressions polynomials appear whose degree characterizes the aberration itself.

The linear terms are usually known as distortions.

Their treatment is made rather complex by simultaneous dependence on the cube of the field angle.

The second degree term represents a focusing error. A good account of this degrading source can be found in [ref. 17] ; the relative transfer function for circular aperture has the expression [ref. 14]

$$T_{op}(f_a) = \frac{4}{\pi} \int_0^{\pi/2} \frac{U \sin U + \cos U - 1}{(C \cos \psi)^2} \, d\psi$$

where

$$U = C \left[(1 - a^2 \sin^2 \psi)^{\frac{1}{2}} - a \cos \psi \right] \cos \psi$$

$$C = \pi (D/F)^2 \, a \, e/\lambda$$

$$a = f_a \, \lambda/D$$

D = lens diameter

F = focal lenght

e = displacement of the detector from the focal plane

Its dependence on the e parameter is shown in fig. A.II.3.

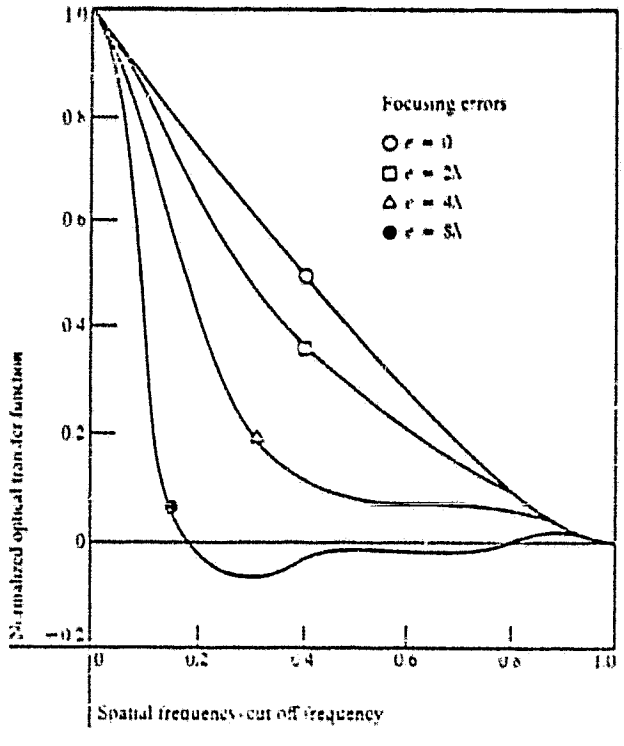

fig. A.II.3

For values e > 2 λ , the function has the sinc trend. The cubic term aberration is the so-called "coma". An example is reported in fig. A.II.4

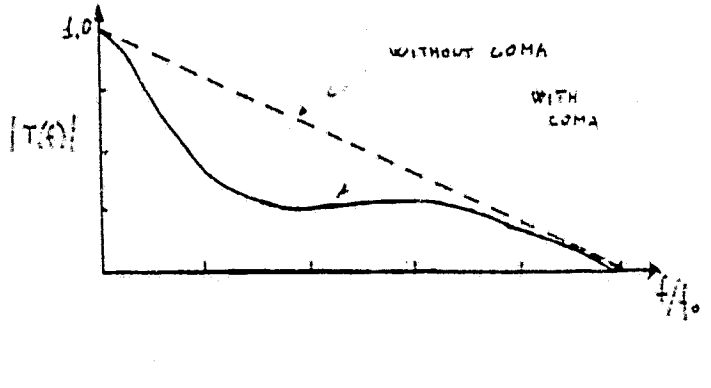

Fig. A.II.4

It must be remembered that the related MTF is no more rotationally invariant as is evident from fig. A.II.5

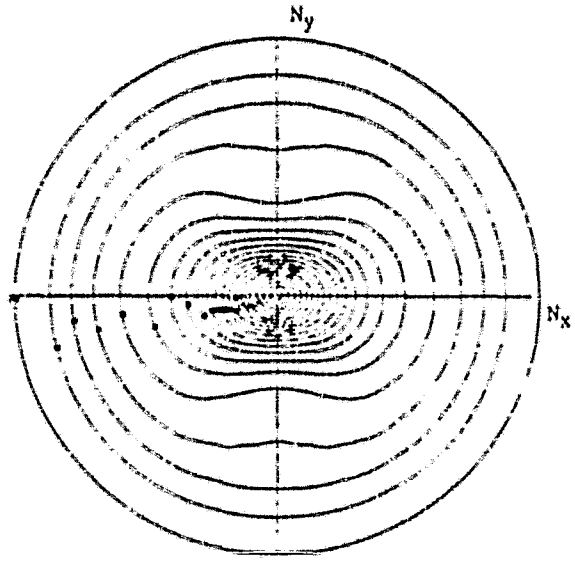

fig. A.II.5

which represents the MTF for a 1λ coma; the equal modulation lines are 0.05 spaced. For an interesting account of these two degradations see [ref. 18] .

The fourth degree term is the spheric aberration.

For their intrinsec nature, the aberrations have space variant PSFs; it follows that for a complete OTF representation, it would be necessary to give separate plots depending on view angle, focal position, wavelength and so on.

It is interesting to note that by using polar coordinates and with a suitable change of variable in r, it is possible to reduce some aberrations (i.e. coma) to linear spatially-invariant degradations [ref. 13, pg. 18] .

- Field-defining system

Under the same use conditions the aperture shape influences the system response as it appears evident from fig. A.II.6.

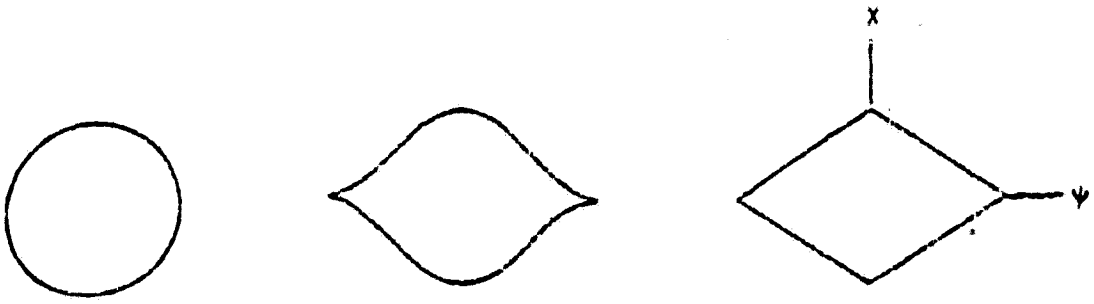

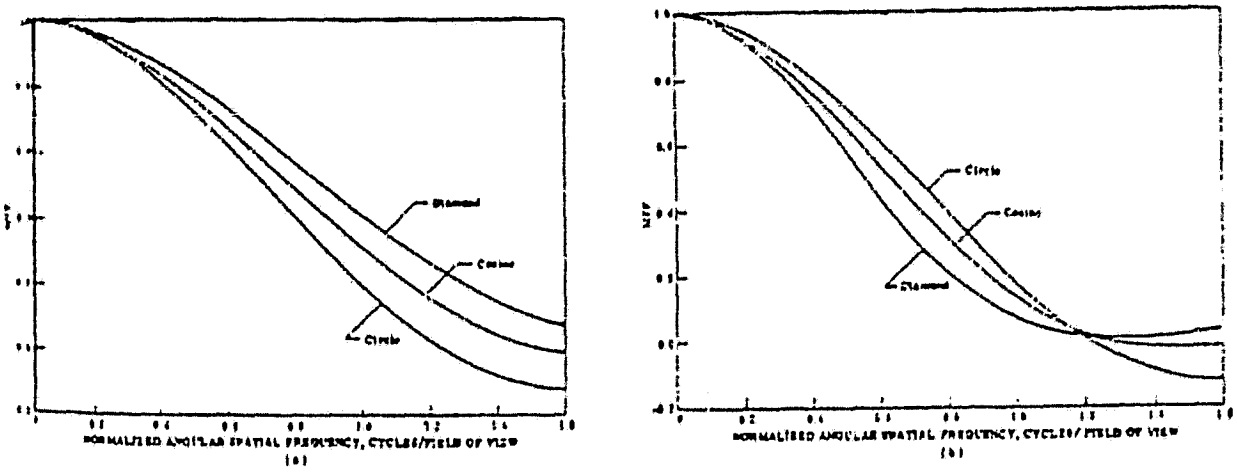

(a) Frequency response section along the line-scan direction, and
(b) normal to the line-scan direction.

fig. A.II.6

- Detecting system and electronics

It must be remembered that electronic system converts a spatial function into a temporal one. Referring only to the f_x case the relation is [ref. 14]

$$f = f_x \, H \dot{\vartheta} \sec^2 \vartheta$$

it follows that detector and electronic characteristics, expressible in terms of temporal frequency transfer functions, influence also spatial frequency MTF.

Since the detecting system can be based upon different physical processes (photo-multiplyers, photodiodes, photoconductors, etc.) also MTF varies depending on the model; an example of MTF derivation is given in [ref. 19 pg. 53] .

- Atmosphere

In respect to the image which would be detected by the sensor in absence of any medium, the presence of the atmosphere produces a blur The effects of this degradation source are of two kinds:

- a radiometric effect coming from scattering, absorption and emission of radiation;
- an effective geometrical blur, representable in the form af a transfer function, caused by atmospheric turbulence.

Examining the latter degradation, it is clear that there is a significant difference for the case of short and long time exposures For the long one, it has been demonstrated that the blurring filter may be approximated by the function $H(u,v) = \exp\left[-C(u^2+v^2)^{5/6}\right]$ where C is a constant depending upon the atmosphere turbolence.

For convenience, the term 5/6 is often replaced by unity so a gaussian curve can be used. A detailed account can be found in the original paper by Hufnagel and Stanley [ref. 20] .

As it appears also from [ref. 14] , in the complete MTF expression there is also an empirical form integral whose numerical value depends from platform altitude.

Among the other degradation sources not still mentioned there are, for example, vibrations and, generally, the motion of the platform. This topic isn't considered here but for a good account of transfer functions coming from image motion see [ref. 14 pg. 37; ref. 16, pg. 436; ref. 21; ref. 22, pg. 101] .

APPENDIX III

LOWPASS FILTERS: SOME EXAMPLES

As it is known, the lowpass filters are characterized by attenuating more the high frequency content of an image than the low frequency one. For the usage these filters are provided for in this work, only filters belonging to the FIR (finite impulse response) class are considered. This means that the impulse response is of finite extent with zero values outside some finite limits.

Furthermore, considering the system is memoryless, the filter output samples must be determined only by input samples i.e. nonrecursive filters are involved. The filters result so to be zero-phase-shift-filters, i.e. they don't alter the phase of the transform.

The unit sample response for many types of two-dimensional filters is of infinite extent; to satisfy then the FIR request, a truncation is needed. Using as truncation function the rectangular one, this results in the introduction in the frequency domain of a percentage of ripple and overshoot. It can be seen that using window functions having in the non-zero region values different from unity, it is possible not only to reduce the error, but also to suitably shape the MTF. A lot of window function can be carried out to project filters as it comes out from [ref. 23 vol. 2 pg 8].

Just as an example the Lanczos-Cappellini window is more closely examined [ref. 7, pg. 65] .
The starting point is the ideal 2-D circularly symmetric low-pass filter with frequency response

$$H(e^{j\omega_1}, e^{j\omega_2}) = \begin{cases} 1 & \sqrt{\omega_1^2 + \omega_2^2} \leq \omega_C \\ 0 & \sqrt{\omega_1^2 + \omega_2^2} > \omega_C \end{cases} \qquad \text{(A.III.1)}$$

where ω_C ($\omega_C = 2\pi f_C$) is the cut frequency shown in fig. A.III.1.

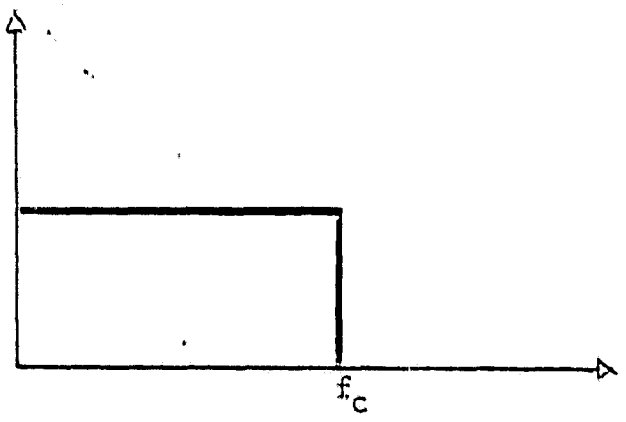

fig. A.III.1

The corresponding discrete impulse response samples are given by

$$h(n_1,n_2) = \alpha \frac{J_1(2\pi\ \alpha\ \sqrt{n_1^2+n_2^2})}{\sqrt{n_1^2 + n_2^2}} \qquad \text{(A.III.2)}$$

where J_1: first order Bessel function

α = normalized frequency f_c/f_s with fs sampling frequency.

This function is clearly not limited and with a noticeable ripple. The window proposed by Lanczos in the one-dimensional case and extended to two-dimensional one by Cappellini is

$$W_L(n_1n_2) = \left(\frac{\sin \frac{\sqrt{2}\ \sqrt{n_1^2 + n_2^2}\ \pi}{N-1}}{\frac{\sqrt{2}\ \sqrt{n_1^2 + n_2^2}\ \pi}{N-1}} \right)^m \qquad \text{A.III.3}$$

where m is a real positive number and

$$n_1,\ n_2 = -\frac{N-1}{2}\ ,\ \ldots,\ \frac{N-1}{2}$$

The final impulse response is then carried out by

multiplying expressions (A.III.2) and (A.III.3). It is interesting to note that changing the set $\{N; \alpha ; m\}$ it is possible to act on MTF characteristic.

An example is given in fig. A.III.2 and fig. A.III.3 where the MTF dependence from respectively, m and N is shown.

The window method is usually implemented in the space domain; it presents however some difficulties as, for example, in determining the impulse transform or to locate the band edges.

An example of filter carried out in frequency domain is the Butterworth lowpass filter (BLPF).

The BLPF of order n and with cut off frequency f_c is defined as

$$H(f) = \frac{1}{1+\left[f/f_c\right]^{2n}} \qquad \text{(A.III.4)}$$

where in the two-dimensional meaning $f = \sqrt{f_x^2 + f_y^2}$. Here the cut-off frequency has no longer the meaning of fig. A.III.1, but it becomes the frequency for which H(f) value corresponds to a certain fraction of its maximum (usually 0.5 or $1/\sqrt{2}$).

One of the main advantages of this filter respect to the former is the possibility of controlling the degree of attenuation in the transition band.

To carry out the discrete version of this filter, the frequency sampling method could be used [ref. 25 §3.2.2.] or another of the techniques described in [ref. 24 §2.5] ; to obtain, however, a filter resembling the BLPF in a manner as simple as possible, the expression (A.III.5) can be used:

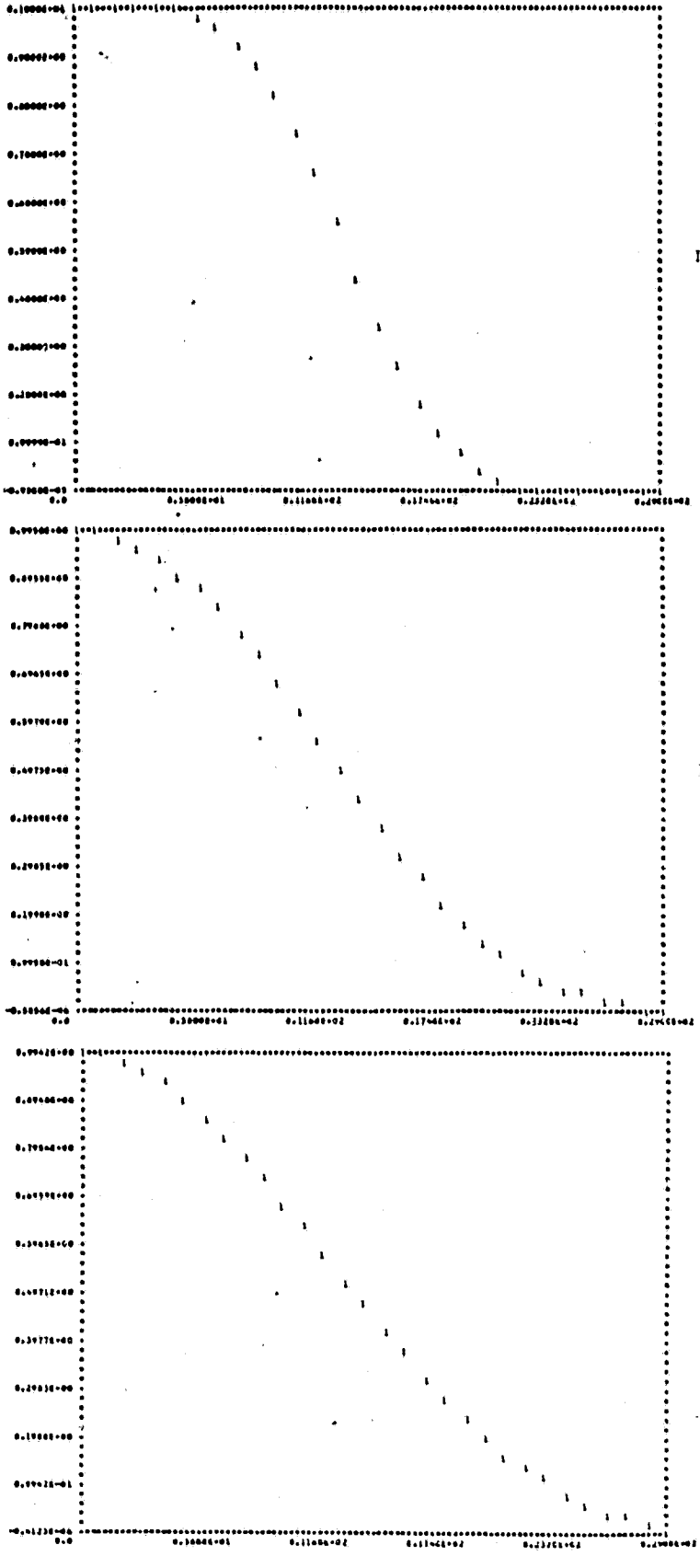

fig. A.III.2.

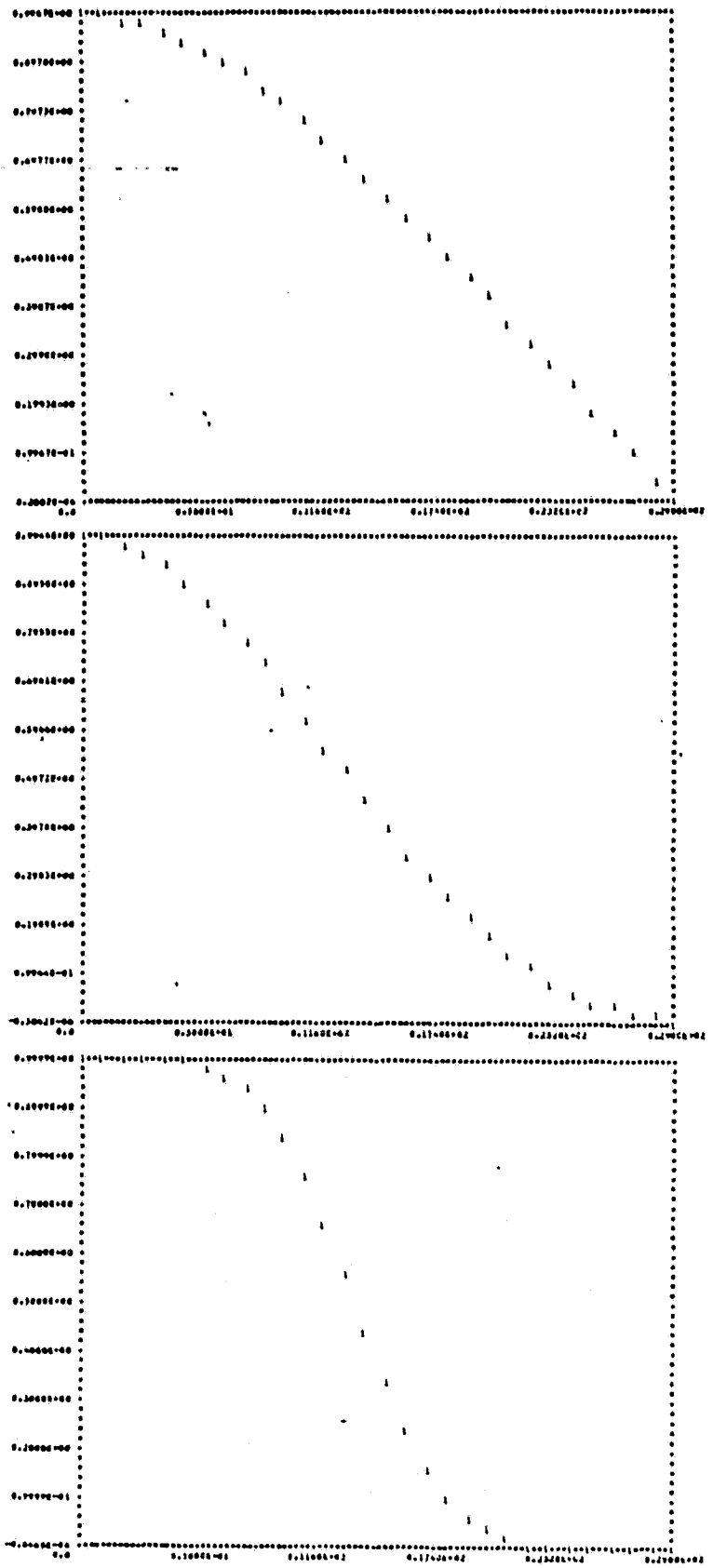

N=8

N=16

N=32

fig. A.III.3.

$$H(n_1,n_2) = \frac{1}{1+\left(\frac{\sqrt{n_1^2 + n_2^2}}{n_{cut}}\right)^{2n}} \qquad \text{(A.III.5)}$$

where $n_{cut} = \frac{f_{cut}}{\Delta f}$ with Δf frequency sampling interval.

The cut-off frequency makes the H value one half of its maximum value.

Fig. A.III.4 shows the trend of this class of filters varying the cut-off frequency while fig. A.III.5 shows the dependence on filter order.

Further examples of filter can be found in [ref. 8 §4.3.2] .

TITOLO

SCALE EFFECTS: HCMM DATA SIMULATION

Usage of filtering techniques for scaling-up simulations

SOMMARIO

A CURA DI

V. Di Gennaro

DATA

Bari, Febbraio 1980

DISTRIBUZIONE

N° RIFERIMENTO

C.S.A.T.A.
Via Amendola, 173
70126 BARI
Tel. (080) 58.33.88